Numerical Analysis of Flow Past a Blunt Heated Cylinder using OpenFOAM

Mohammed Saqlain

UG Student, Department of Mechanical Engineering
The National Institute of Engineering, Mysore 570008

Abstract –

This study presents a comprehensive transient numerical analysis of the flow and heat transfer characteristics of flow past a 2D blunt heated cylinder using the open-source computational fluid dynamics (CFD) software OpenFOAM. This study focuses on the numerical analysis of flow over a blunt heated cylinder and investigates its heat transfer characteristics using chtMultiRegionFoam in openFOAM. A range of Reynolds numbers *10,000 < Re <100,000* was considered in the simulation. The analysis involved examining various parameters such as lift and drag coefficients, Nusselt number, Strouhal number, and the variation of pressure, temperature, and velocity contours. The results revealed interesting trends and phenomena. The lift and drag coefficients exhibited fluctuations at higher Reynolds numbers, indicating flow unsteadiness and turbulence effects. The Nusselt number provided insights into the heat transfer between the cylinder and the fluid stream, while the Strouhal number highlighted the shedding of vortices in the wake region. The pressure, temperature, and velocity contours offered a visual representation of the flow characteristics. Overall, this study enhances our understanding of the flow behaviour and heat transfer in the context of a blunt heated cylinder, contributing to the broader knowledge in fluid dynamics and thermal sciences.

1. Introduction

Kawaguti, in 1953, achieved the earliest numerical solution for flow around a cylinder through extensive manual calculations, which demanded significant labor and endurance over an extended period of time. However, with the advent of modern computational techniques, it is now possible to simulate and obtain results for similar problems within a much shorter timeframe. The study of external flows around objects has gained significant attention due to its practical applications. For instance, the streamlined shapes of airfoils are designed to

maximize lift and minimize aerodynamic drag on wings. Conversely, the flow around bluff bodies, such as circular cylinders, typically involves the separation of boundary layers and the occurrence of strong flow oscillations in the wake region. In certain Reynolds number ranges, the shedding of vortices alternately from each side of the cylinder leads to the formation of a periodic pattern known as a Karman vortex street. This phenomenon generates an oscillating flow at a specific frequency directly linked to the Reynolds number of the flow. The periodic nature of vortex shedding can sometimes induce undesirable structural vibrations, particularly when the shedding frequency coincides with one of the resonant frequencies of the structure. A well-known example illustrating these effects is the Tacoma Narrows bridge incident [1]

Fig 1 - Flow induced vibration caused the Tacoma Narrows Bridge to experience vertical and torsional vibrations leading to its collapse 1940 [1]

Understanding the behavior of fluid flow around bluff bodies and investigating the associated convective heat transfer characteristics are essential in numerous engineering applications. Bluff bodies, characterized by their rounded and blunt shape, commonly encounter flow separation, recirculation zones, and complex flow patterns. The study of flow past bluff bodies plays a crucial role in optimizing the performance of various systems, including heat exchangers, cooling systems, and aerodynamic designs.

The present research focuses specifically on the flow past a blunt heated cylinder, which represents a common and practical scenario encountered in many engineering applications. Blunt cylinders are widely used in heat transfer systems, such as nuclear reactor cores, industrial chimneys, and chemical reactors, where convective heat transfer is of paramount

importance. Analyzing the flow and heat transfer characteristics of flow past a blunt heated cylinder offers valuable insights into the behavior of the system and aids in optimizing its performance.

The study of flow past a blunt heated cylinder involves investigating both the aerodynamic forces acting on the cylinder and the convective heat transfer phenomena associated with it. The lift and drag coefficients, which represent the aerodynamic forces, directly affect the stability, efficiency, and maneuverability of the cylinder. Understanding these forces is crucial for designing systems that require controlled fluid flow and minimized drag, such as vehicles, buildings, and industrial equipment. Moreover, convective heat transfer characteristics play a vital role in determining the thermal performance of the system. The heat transfer efficiency around the blunt heated cylinder is quantified using the Nusselt number, which provides valuable information about the convective heat transfer coefficient. Accurate prediction and analysis of the Nusselt number enable the optimization of heat transfer systems, leading to improved energy efficiency and enhanced thermal management.

Extensive research has been conducted to gain a comprehensive understanding of fluid flow around cylinders with circular, semicircular, square, and triangular cross sections. Such studies are crucial due to the diverse range of fluid flow phenomena associated with these shapes. The dynamics of wake formation and vortex generation behind these simplified shapes hold significant practical importance in engineering. However, there has been limited focus on analyzing the flow and heat transfer characteristics around more complex geometries, such as a blunt-headed body, which is increasingly utilized in various industries. Flow past bluff bodies finds typical application in industries involving heat exchange, material processing, cooling systems, construction, oil and gas transportation, combustion chambers, chimney stacks, electronic cooling devices, measurement instruments, nuclear reactor cooling, flow measurement, and distribution systems.

In conclusion, studying the flow and heat transfer characteristics of flow past a blunt heated cylinder holds significant importance in various engineering fields. The analysis of aerodynamic forces, convective heat transfer phenomena, and the associated parameters, such as lift and drag coefficients and Nusselt number, provides valuable insights for optimizing the performance of heat transfer systems. By focusing on the practical application of studying the behavior of flow past a bluff body, specifically the blunt heated cylinder, this research aims to contribute to the advancement of thermal engineering and enhance the efficiency and reliability of related systems.

1.1 Flow over bluff body

Studying flow over bluff bodies is significant in various fields of science and engineering. Bluff bodies are objects or geometries that have a substantial impact on fluid flow due to their shape, resulting in complex flow patterns and phenomena. Here are some key reasons why studying flow over bluff bodies is important:

i.   **Drag and Lift Forces:** Bluff bodies experience drag and lift forces due to the flow around them. Understanding the flow characteristics helps in predicting and managing these forces, which is crucial for designing aerodynamic structures, vehicles, and objects that need to overcome resistance and achieve desired motion or stability. By studying flow patterns and optimizing the shape of bluff bodies, it is possible to minimize drag and maximize lift, improving the efficiency and performance of various applications.

ii.   **Aerodynamics and Vehicle Design:** Bluff bodies are encountered in the design of aircraft, automobiles, trains, buildings, and other structures. Studying the flow behavior around these bodies helps in optimizing their design, reducing aerodynamic drag, and improving fuel efficiency. By analyzing flow separation, boundary layer development, and vortices generated by bluff bodies, engineers can make informed design decisions, leading to improved vehicle performance, stability, and reduced energy consumption.

iii.   **Energy Generation and Renewable Resources:** Bluff bodies play a crucial role in the design of energy generation systems. Wind turbines, for example, utilize bluff body aerodynamics to extract energy from wind flow. Understanding the flow behavior around the blades and tower aids in optimizing the turbine design, enhancing power output, and improving the efficiency of renewable energy conversion. Similar considerations apply to hydroelectric turbines and other energy harvesting systems.

iv.   **Heat Transfer and Thermal Management:** Flow over bluff bodies influences heat transfer characteristics. Understanding the flow patterns and heat transfer mechanisms is important for applications such as cooling electronic components, optimizing heat exchangers, and designing efficient thermal management systems. By studying the flow behavior, researchers and engineers can develop effective cooling strategies, improve thermal efficiency, and prevent overheating in various industrial and electronic systems.

v.   **Environmental and Civil Engineering:** Flow over bluff bodies plays a role in environmental and civil engineering applications. For instance, studying flow patterns

around buildings can help optimize urban planning, reduce wind-induced loads on structures, and enhance pedestrian comfort. Understanding flow around bridges and offshore structures helps in designing stable and resilient infrastructure. Additionally, analyzing flow over coastal structures aids in coastal engineering, erosion control, and the development of sustainable coastal protection measures.

Overall, studying flow over bluff bodies is essential for understanding and optimizing various engineering systems and natural phenomena. It enables the design of efficient and safe structures, enhances energy conversion and thermal management, and contributes to advancements in aerospace, automotive, renewable energy, environmental, and civil engineering fields.

1.2 Literature Review

The following literatures [2–6] contain recent investigations on forced convective flows through square and semicircular cylinders in two-dimensional laminar flow regime. For instance, Sahu et al.'s [2] numerical analysis of the impact of the Reynolds and Prandtl numbers on the rate of heat transfer from a square cylinder under a variety of conditions is presented in his work. In the two-dimensional regime, for Reynolds numbers ranging from $1 < Re < 160$, Sharma et al. [3] published their numerical work on the flow structure and heat transfer characteristics of an isolated square cylinder in cross flow for both steady and unsteady periodic laminar flow. The impact of vortex shedding on the isotherm patterns and heat transport from the cylinder is clarified by their analysis. In a separate study, Dhiman et al. [4] investigated the flow and heat transfer properties of a symmetrically positioned square cylinder in cross-flow over a range of Reynolds, Prandtl, and blockage ratios. Paliwal et al. [5] and Gupta et al. [6] have explored the impact of the Prandtl number on the heat transfer from unconfined and confined square cylinders in a constant flow environment. The force convective flow and heat transfer characteristics via an unconfined blunt-headed cylinder have been calculated for a range of Reynolds $10 < Re < 200$ and Prandtl $0.7 < Pr < 100$ numbers has been reported by H. Kapadia et al. [7].

Therefore, it is conceivably safe to conclude that no prior work is available on the influence of Reynolds number of range $10000 < Re < 100000$ and Prandtl numbers considering the working fluid (air) temperature $T = 300$ k. This research aims to fill this gap in the literature. Therefore, in the present numerical investigation, the effects of Reynolds number and Prandtl number on

the characteristics of fluid flow and heat transfer under forced convection past a blunt headed cylinder has been studied using the open source CFD tool, openFOAM.

1.3 Fluid flow and Heat transfer parameters

Fluid flow and heat transfer parameters play a crucial role in understanding and analyzing the behavior of fluid flow and heat transfer processes. In the context of present study, various non-dimensional numbers and Coefficients have been analyzed. The details which are as given below.

1.3.1 Reynolds Number

The Reynolds number is a dimensionless parameter used in fluid mechanics to characterize the flow regime of a fluid and predict the transition from laminar to turbulent flow. It is named after the Irish engineer Osborne Reynolds, who first studied the phenomenon of fluid flow.

The Reynolds number (Re) is defined as the ratio of inertial forces to viscous forces within a fluid flow. It is calculated using the following formula:

$$R_e = \frac{\rho\, U\, L}{\mu}$$

Where, ρ, U and L is the density, velocity and characteristic length scale of the fluid and μ is the dynamic viscosity of the fluid.

The Reynolds number is an important parameter as it determines the flow regime and provides information about the behaviour of the fluid flow. It helps in understanding how the fluid will behave, whether it will have a smooth, orderly laminar flow or a chaotic, turbulent flow. The Reynolds number affects the convective heat transfer coefficient. The transition from laminar to turbulent flow can significantly impact the heat transfer rates and efficiency of heat exchangers and other heat transfer devices. In the study of flow around bluff body, the Reynolds number helps determine the flow regime and influences drag, lift, and other aerodynamic characteristics.

1.3.2 Lift and Drag Coefficients

In the field of fluid dynamics, drag refers to a force that acts in the opposite direction or counteracts the relative movement of a mass within a fluid environment. This phenomenon occurs when there is motion between two layers of fluid, two surfaces, or a fluid and a solid surface. Unlike other resistance forces, like dry friction, which remain relatively constant

regardless of speed, drag forces vary depending on the velocity. In the case of a smooth flow, the drag force is directly proportional to the velocity, while in a turbulent flow, the drag force is proportional to the square of the velocity. Although the primary cause of drag is related to viscous friction, turbulent drag does not rely on the viscosity of the fluid.

The drag coefficient (Cd) is a dimensionless coefficient that is used to describe the drag or resistance experienced by an object moving through a fluid. The drag coefficient is defined as the ratio of the drag force acting on an object to the dynamic pressure of the fluid times the reference area. The drag coefficient is generally determined by experiments and depends on the fluid flow conditions and the shape of the object. For example, a streamlined object with a smooth surface will have a lower drag coefficient than a rough or irregular object.

The drag coefficient is given by:

$$C_d = \frac{F_D}{0.5\,\rho\,U_\infty^2\,D}$$

Lift force is the upward force that opposes the weight of an object and acts perpendicular to the direction of motion. It is caused by the difference in air pressure above and below an object, such as an airplane wing or a kite. The shape of the object, its velocity, and the density and viscosity of the fluid it is moving through all affect the amount of lift force generated. The lift force is generally caused by the Bernoulli's principle, which states that as the velocity of a fluid increases, its pressure decreases. The curved upper surface of a wing is designed to create a greater velocity of air over the top of the wing, which results in a lower pressure area above the wing and generates lift force.

The lift coefficient (Cl) is a dimensionless coefficient that is used to describe the lift force experienced by an object moving through a fluid. It is commonly used in fluid dynamics and aerodynamics to quantify the lift force experienced by an object as it moves through a fluid. The lift coefficient is defined as the ratio of the lift force acting on an object to the dynamic pressure of the fluid times the reference area.

$$C_l = \frac{F_l}{0.5\,\rho\,U_\infty^2\,D}$$

Where, F_D is the drag force, C_d is dragging coefficient, ρ is density of the fluid, U is velocity of the fluid or object, D referred to reference area or characteristic length and F_l and C_l are the drag force & drag coefficient respectively.

1.3.3 Strouhal Number

The Strouhal number is a dimensionless parameter used in fluid dynamics to characterize the unsteady behaviour of fluid flow around an object. It relates the frequency of vortex shedding or oscillations in the flow to the flow velocity and a characteristic length scale of the object. The Strouhal number is named after the Czech physicist Vincenc Strouhal, who first observed the relationship between frequency and flow characteristics.

Mathematically, the Strouhal number (St) is defined as:

$$C_l = \frac{f\,L}{U}$$

Where, f is the frequency of vortex shedding or oscillations in the flow, L is a characteristic length scale of the object, such as the diameter or width. U is the flow velocity.

The Strouhal number provides important insights into the unsteady behaviour of fluid flow and is particularly relevant for flows around bluff bodies, such as cylinders or aerofoils. It is often used to predict the occurrence of flow-induced vibrations, acoustic phenomena, or the shedding of vortices behind the object.

1.3.4 Nusselt Number

The Nusselt number is a dimensionless parameter used in the field of heat transfer to quantify the convective heat transfer rate from a heated surface. It represents the ratio of convective heat transfer to conductive heat transfer between a solid surface and a fluid. The Nusselt number is named after Wilhelm Nusselt, a German engineer who made significant contributions to the study of heat transfer.

Mathematically, the Nusselt number (Nu) is defined as:

$$Nu = \frac{h\,L}{k}$$

Where, h is the convective heat transfer coefficient, which characterizes the heat transfer rate between the solid surface and the fluid. L is a characteristic length scale of the system, such as the length of the heated surface, k is the thermal conductivity of the fluid.

1.3.5 Heat Transfer Coefficient

The heat transfer coefficient is a key parameter in heat transfer analysis, representing the rate of heat transfer between a solid surface and a fluid medium. It quantifies the effectiveness of convection in transferring thermal energy. The heat transfer coefficient (h) is defined as the

amount of heat energy transferred per unit time, per unit area, and per unit temperature difference between the surface and the fluid. It is expressed in units of watts per square meter-kelvin (W/(m²·K)).

Mathematically,

$$h = \frac{q}{A \times \Delta T}$$

where, q is the rate of heat transfer, A is the surface area in contact with the fluid, ΔT is the temperature difference between the surface and the fluid.

The heat transfer coefficient depends on fluid properties, flow conditions, and surface characteristics. Factors such as thermal conductivity, viscosity, flow velocity, flow regime, surface roughness, and geometry influence the heat transfer coefficient. Higher flow velocities and turbulent flow promote enhanced convective heat transfer. Smooth surfaces generally promote better heat transfer. The heat transfer coefficient may vary along the surface and can be determined through experimental measurements, empirical correlations, or computational fluid dynamics simulations. Accurate knowledge of the heat transfer coefficient is important for designing and analyzing heat transfer systems, optimizing performance, and ensuring efficient heat transfer between solids and fluids.

2. Problem Statement

The present study aims to perform a comprehensive transient numerical analysis of flow and heat transfer characteristics over a 2D blunt heated cylinder using the open-source computational fluid dynamics (CFD) software OpenFOAM. The investigation focuses on understanding the flow behaviour and heat transfer properties of the cylinder in different operating conditions. A range of Reynolds numbers *10,000 < Re <100,000* was considered in the simulation. The analysis involved examining various parameters such as lift and drag coefficients, Nusselt number, Strouhal number, and the variation of pressure, temperature, and velocity contours.

3. Governing Equations

It is assumed that the fluid flow is turbulent, two-dimensional and unsteady. Though the flow velocity is very less to constitute a large variation in density of the working fluid yet it is considered to be compressible in nature. The SST k-ω turbulence model is put into application, The k-omega SST (Shear Stress Transport) model is a popular Reynolds-Averaged Navier-

Stokes (RANS) turbulence model that combines aspects of both the k-epsilon and k-omega models. It offers improved predictions for a wide range of flows, including both attached and separated turbulent boundary layers. The fluid's physical characteristics, including viscosity and density, as well as its thermal characteristics, including heat capacity and thermal conductivity, are taken for granted to remain constant. The flow and energy equations are independently solved in the current work. We can disregard the modification of the aforementioned fluid properties with temperature since the maximum temperature difference between the incoming fluid and heated blunt headed body is kept very minimal. The governing differential equations is given as follows.

Conservation of Mass (Continuity Equation):

$$\frac{\partial \rho}{\partial t} + \frac{\partial(\rho U)}{\partial x} + \frac{\partial(\rho V)}{\partial y} = 0 \qquad\qquad\text{--- (1)}$$

Conservation of Momentum (Momentum Equations):

X -momentum –

$$\frac{\partial(\rho U)}{\partial t} + U\frac{\partial(\rho U)}{\partial x} + V\frac{\partial(\rho U)}{\partial y} = -\frac{\partial P}{\partial x} + \mu_{eff}\left(\frac{\partial^2 U}{\partial x^2} + \frac{\partial^2 U}{\partial y^2}\right) + \rho g_x \qquad\text{--- (2)}$$

Y -momentum –

$$\frac{\partial(\rho V)}{\partial t} + U\frac{\partial(\rho V)}{\partial x} + V\frac{\partial(\rho V)}{\partial y} = -\frac{\partial P}{\partial y} + \mu_{eff}\left(\frac{\partial^2 V}{\partial x^2} + \frac{\partial^2 V}{\partial y^2}\right) + \rho g_y \qquad\text{--- (3)}$$

Energy Equation:

$$\frac{\partial(\rho E)}{\partial t} + \frac{\partial(\rho U H)}{\partial x} + \frac{\partial(\rho V H)}{\partial y} = -\frac{\partial(PU)}{\partial x} - \frac{\partial(PV)}{\partial y} + k\left(\frac{\partial^2 T}{\partial x^2} + \frac{\partial^2 T}{\partial y^2}\right) + Q \qquad\text{--- (4)}$$

Turbulence Model Equations (k-omega SST RANS):

Transport Equation for Turbulent Kinetic Energy (k) –

$$\frac{\partial(\rho k)}{\partial t} + \frac{\partial(\rho k U)}{\partial x} + \frac{\partial(\rho k V)}{\partial y} = \frac{\partial}{\partial x}\left[\left(\mu + \frac{\mu_t}{\sigma_k}\right)\frac{\partial k}{\partial x}\right] + \frac{\partial}{\partial y}\left[\left(\mu + \frac{\mu_t}{\sigma_k}\right)\frac{\partial k}{\partial y}\right] + P_k - \beta\rho k\omega \qquad\text{--- (5)}$$

Transport Equation for Specific Dissipation Rate (ω) –

$$\frac{\partial(\rho\omega)}{\partial t} + \frac{\partial(\rho\omega U)}{\partial x} + \frac{\partial(\rho\omega V)}{\partial y} = \frac{\partial}{\partial x}\left[\left(\mu + \frac{\mu_t}{\sigma_\omega}\right)\frac{\partial\omega}{\partial x}\right] + \frac{\partial}{\partial y}\left[\left(\mu + \frac{\mu_t}{\sigma_\omega}\right)\frac{\partial\omega}{\partial y}\right]$$

$$+ \alpha P_k - \beta\rho\omega^2 + 2(1 - \text{F1})\frac{\rho\sigma}{\omega} \qquad\text{--- (6)}$$

Where, ρ is the density of air, t is the time, (u, v) are the velocity components in the x and y directions, respectively. p is the pressure. μ_{eff} is the effective viscosity, which combines molecular viscosity and the turbulent viscosity. g_x and g_y are the acceleration components in the x and y directions, respectively. E is the total energy per unit volume, k is the turbulent kinetic energy, ω is the specific dissipation rate. P_k represents the production of turbulent kinetic energy, β is the model constants, μ_t is the turbulent viscosity, F1 An empirical blending function used to transition between different regions of the flow (typically based on flow conditions or distance from the wall). And σ is Turbulent Prandtl number related to the diffusion of ω and k.

4. Simulation Procedure

4.1 Geometry and Mesh

The geometry with the empirical dimensions is as shown in figure and meshing as shown in Figure 2. A fixed, two-dimensional, blunt-headed entity is immersed in a constant free-stream flow of velocity U. The blunt-headed bluff body has a diameter of D and a length of 1.5D. The domain is 35D in length and 20D in height. Upstream length is 8D, whereas downstream length is maintained at around 27D. The geometric center of the circular section of the blunt-headed body serves as the origin of coordinates, with drag force positive in the positive x-direction and lift force positive in the positive y-direction.

The blockMesh is a mesh generation utility in OpenFOAM that creates structured meshes for CFD simulations. It uses a Cartesian coordinate system to define the geometry and mesh of the computational domain. The mesh consists of hexahedral cells arranged in a regular grid pattern. By defining blocks and their vertices or sizes, complex geometries can be created. Boundary conditions can be assigned to define flow conditions. Mesh refinement is possible through sub-blocking and grading factors. Quality control features ensure mesh orthogonality, aspect ratio, and skewness. The generated mesh can be visualized and used for accurate and efficient CFD simulations. Overall, blockMesh is a versatile tool that enables the creation of high-quality structured meshes for a wide range of geometries and flow problems.

It has been utilized in the present study for creating geometry and discretization of the physical domain. The code for which is given in Annexure 1 and the Mesh is as shown in Figure 3. The mesh has a total of 94400 hexahedral cells and 45.013766 of max. aspect ratio with 1.5506776 of max. skewness. The present mesh has been adopted after a grid independent study and comparing 7 different mesh size which has been discussed in *Article 6.*
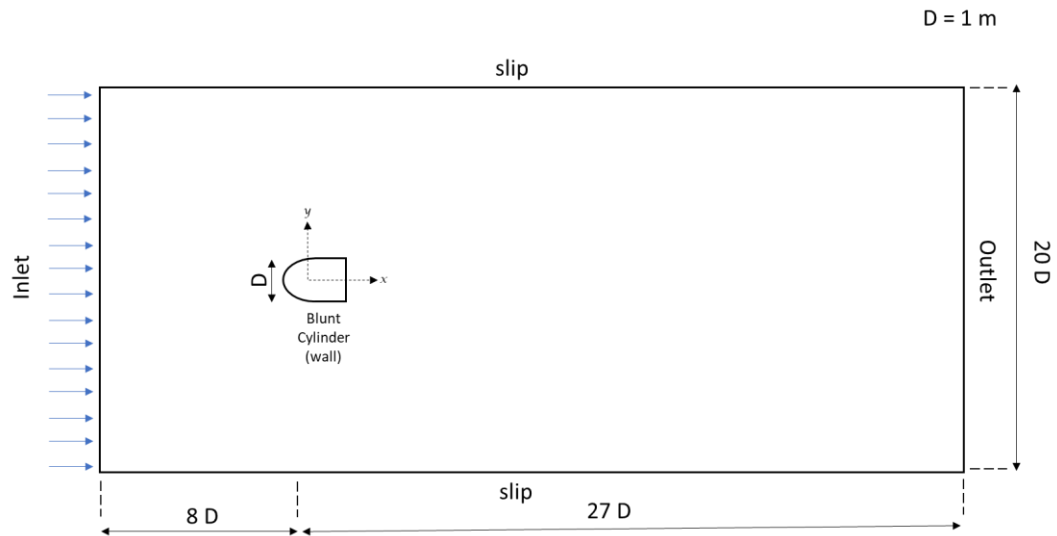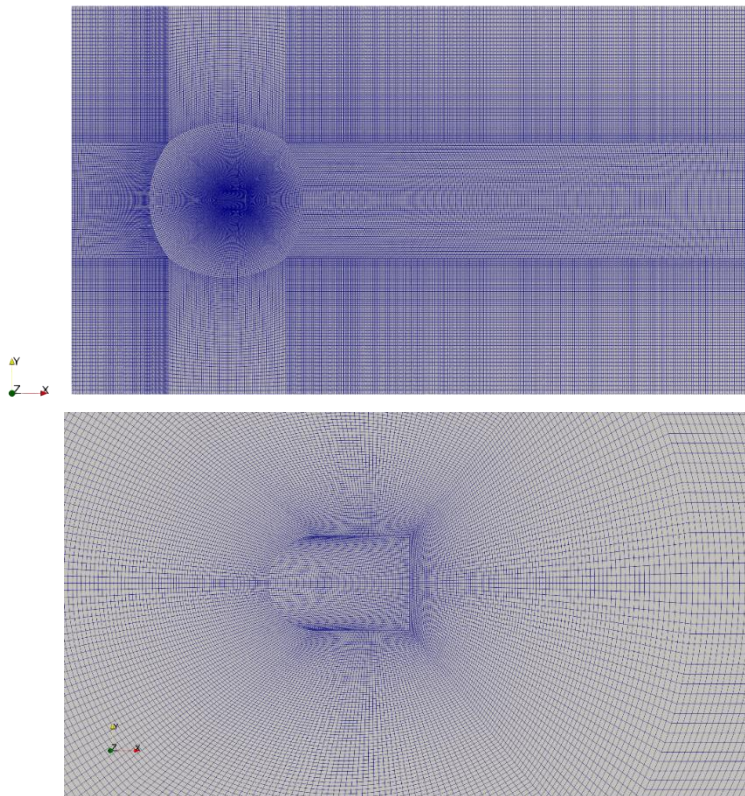

Fig 2 - Physical domain for present study

Fig 3 – Mesh full view (top) and zoomed view (bottom)

4.1.1 topoSet utility and STL File:

The topoSetDict file is located in the system folder of the case directory. It is a plain text file written in the OpenFOAM dictionary format. It consists of sections enclosed in curly braces { } and contains key-value pairs or sub-dictionaries.

The main sections typically found in topoSetDict are:

- **actions:** This section defines the actions to be performed on cell sets. Each action is specified as a sub-dictionary with a unique name. Common actions include creating, merging, subtracting, or intersecting cell sets.
- **setFormat:** This section specifies the format of the cell set file that will be generated by the actions. It defines the file format and optionally specifies the fields to be included.
- **regions:** This section defines the initial regions or cell sets before any actions are performed. Each region is specified as a sub-dictionary with a unique name. The region can be defined based on various criteria such as cell indices, geometric shapes, or other pre-defined cell sets.

The topoSetDict file allows you to manipulate cell sets dynamically during the simulation or pre-processing stages. By defining and performing various actions on cell sets, we can control the behavior and properties of different regions within our computational domain.
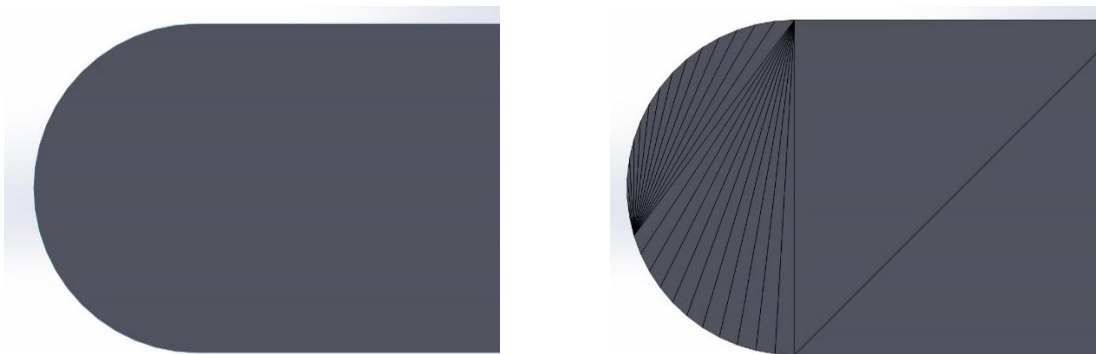
Fig 4 – Blunt cylinder geometry plain surface (left) and stl image (right)

The STL (Standard Tessellation Language) file holds significant importance in the topoSet dictionary of OpenFOAM as it serves as the basis for defining specific regions or cell sets within the computational domain. By utilizing the geometry information stored in the STL file, topoSet enables the creation and manipulation of cell sets based on the defined geometric shapes. These cell sets play a crucial role in tasks such as applying boundary conditions, performing post-processing analysis, or extracting data from specific regions of interest within

the simulation. The STL file serves as the bridge between the geometric representation of the object or surface and the cell sets used for further analysis and manipulation in OpenFOAM simulations. In the present study, STL file for the solid blunt cylinder is created using solidWorks and imported in *constant/triSurface/<file>. stl*

Figure 4 depicts the STL file of solid blunt cylinder and code for topoSet is given Annexure 3.

Note: It was observed that when, STL file and blockMesh file is visualized together in paraView, there was deviation of (0.5 0.5 0) between STL and blockMesh file as depicted in Figure 5. Therefore, a preprocess utility transformPoints has been used to counter this issue.

```
transformPoints "translate=(0.5 0.5 0)"
```
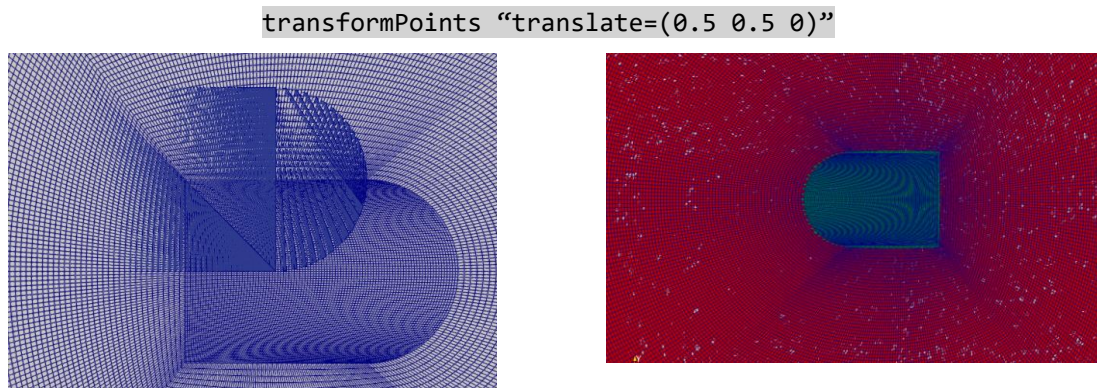

Fig 5 – Before (left) and after (right) of using transformPoints utility function.

4.2 Initial and Boundary Conditions

The initial and boundary conditions for the present problem are as listed in the Table 1:

Table 1 - Boundary Conditions

Boundary Condition	region	patch	type	value
P	fluid	inlet	calculated	uniform 100000
		outlet	calculated	uniform 100000
		topAndBottom	zeroGradient	-
		wall	zeroGradient	-
U	fluid	inlet	fixedValue	uniform (u 0 0)
		outlet	pressureInletOutletVelocity	uniform (0 0 0)
		topAndBottom	slip	-
		wall	noslip	-
T	fluid	inlet	fixedValue	uniform 300
		outlet	inletOutlet	uniform 300
		topAndBottom	zeroGradient	-
		wall	compressible::turbulentTemperatureCoupledBaffleMixed;	uniform 300
T	solid	wall	compressible::turbulentTemperatureCoupledBaffleMixed;	uniform 300

The *"slip"* condition sets the value of the normal component of the velocity to zero and allows the tangential component to vary freely. On the surface of the blunt headed shaped object: Constant heat flux = 1000 w/m^2 and initial condition T = 350K. At the outlet boundary the

"zeroGradient" condition is applied. This condition assumes that the pressure gradient at the outlet as zero.

4.3 chtMultiRegionFoam solver

The chtMultiRegionFoam solver in OpenFOAM is specifically designed for simulating fluid flow and heat transfer problems involving multiple interacting regions or domains. It is commonly used to study complex phenomena where heat transfer occurs across different materials or regions with distinct properties.

Here are some applications of chtMultiRegionFoam in the domain of fluid flow and heat transfer:

i.   Conjugate Heat Transfer (CHT): chtMultiRegionFoam is extensively used for simulating CHT problems, where the heat transfer between fluid and solid regions is considered. It allows for the analysis of various configurations such as heated walls, cooling channels, and immersed objects within a fluid domain. Such simulations are vital in industries such as aerospace, automotive, and power generation, where accurate prediction of temperature distribution and heat transfer rates is crucial.

ii. Electronics Cooling: The solver is employed in the study of cooling electronic components, such as heat sinks, printed circuit boards (PCBs), and electronic packages. By considering both the fluid region (air or coolant) and solid regions (electronic components), chtMultiRegionFoam enables the investigation of temperature distribution, convective heat transfer, and the effectiveness of cooling strategies to optimize the thermal management of electronic devices.

iii. Industrial Processes: chtMultiRegionFoam finds application in various industrial processes involving fluid flow and heat transfer. For instance, it can be used to model heat exchangers, where multiple regions represent different fluid streams, allowing the analysis of temperature profiles, heat transfer rates, and pressure drops across the exchanger. It is also employed in simulating cooling of industrial machinery, chemical reactors, and other equipment where accurate thermal analysis is crucial.

iv. Renewable Energy Systems: The solver is valuable in simulating renewable energy systems, such as solar thermal collectors and geothermal systems. It enables the investigation of fluid flow, convective heat transfer, and the overall efficiency of the systems. By considering the interaction between the fluid and solid regions,

chtMultiRegionFoam assists in optimizing the design and performance of these energy conversion systems.

Overall, chtMultiRegionFoam facilitates the analysis of problems involving fluid flow and heat transfer across multiple interacting regions. By considering the thermal interaction between fluid and solid domains, it allows for a comprehensive study of phenomena, enabling engineers and researchers to gain insights into complex heat transfer processes and optimize system performance in various applications.

4.3.1 Case Setup in chtMultiRegionFoam

```
0/: folder
      | ------------     fluid/: folder
                              |-------------  -  alphat
                                              -  k
                                              -  nut
                                              -  omega
                                              -  p
                                              -  p_rgh
                                              -  T
                                              -  U
      | ------------     solid/: folder
                              |-------------  -  T
constant/: folder
      | -----    fluid/: folder
                              |-------------  -  g
                                              -  momentumTransport
                                              -  physicalProperties
                                              -  pRef
                                              -  thermophysicalTransport
                                              -  polyMesh/: folder
      | -----    solid/: folder
                              |-------------  -  fvModels
                                              -  physicalProperties
                         polyMesh/: folder
                              |-------------  -  boundary
                                              -  cellZones
                                              -  faces
                                              -  neighbour
                                              -  owner
                                              -  points
                                              -  sets/: folder
      | -----    triSurface/: folder
                              |-------------  -  STL file
      | -----    regionProperties
system/: folder
      | -----    fluid/: folder
                              |-------------  -  fvSchemes
                                              -  fvSolution
      | -----    solid/: folder
                              |-------------  -  fvSchemes
                                              -  fvSolution
      | -----    blockMeshDict
      | -----    controlDict
      | -----    fvSchemes
      | -----    fvSolution
      | -----    topoSetDict
```

Fig 6 - Folder structure of chtMultiRegionFoam solver in openFOAM V10.

The present study which involves OpenFOAM v10, the chtMultiRegionFoam solver is used for simulating conjugate heat transfer problems involving multiple fluid regions. Here are the details of each folder typically associated with the chtMultiRegionFoam solver in OpenFOAM v10:

The *"0"* folder holds the initial conditions for the simulation. It typically includes files like, *"p"* for Initial pressure field, *"T"* for Initial temperature field, *"u"* for Initial velocity field *"k"* and *"omega"* (if using a turbulence model): Initial turbulence kinetic energy and dissipation rate fields.

"constant" folder contains various files related to the problem's constant properties and boundary conditions. Some important files are like *"transportProperties"* to Specifies the transport model and properties of the fluid regions. *"thermophysicalProperties"* Defines the thermophysical properties (e.g., density, viscosity, thermal conductivity) of the fluid regions. The *"polyMesh"* folder contains the mesh files used for the simulation. It includes files like *"boundary"* to define the boundary patches and their types. *"cellZones"* to specify the different cell zones or regions in the domain. *"faces", "neighbour", "owner"* are the files defining the face-face, face-cell, and cell-cell connectivity of the mesh and *"points"* defines coordinates of mesh vertices. The *"regionProperties"* files specifies the region type of each region in the simulation. i.e., solid or fluid, based on which the specific properties of each region will be specified in this folder.

The *"system"* folder contains the main configuration files for the simulation. Key files include *"controlDict"* which Defines the simulation control parameters such as start/end time, time step size, and output intervals etc. the *"fvSchemes"* and *"fvSolution"* files to specify the numerical schemes and solvers used for the simulation. the *"topoSetDict"* file is used to define and manipulate cell sets or regions within the computational domain. These cell sets can be used for various purposes, such as specifying regions where specific boundary conditions should be applied, defining regions for post-processing, or identifying regions for advanced mesh manipulation operations.

The *"postProcessing"* folder is created during the simulation and contains various sub-folders for post-processing the simulation results.

4.3.2 Courant number in CFD simulations

In computational fluid dynamics (CFD), the Courant number (also known as the CFL number) is a dimensionless parameter used to characterize the stability and accuracy of numerical methods for solving the governing equations of fluid flow. It is named after the French mathematician Maurice Courant.

The Courant number is defined as the ratio of the local convective time step to the local physical time step. It is given by the formula:

$$C = \frac{u \times \Delta t}{\Delta x}$$

Where, C is the Courant number. u is the local velocity magnitude or the maximum velocity in the computational domain. Δt is the time step used in the simulation. Δx is the grid spacing or characteristic length in the computational domain.

The Courant number is a measure of how far a fluid element can move during a single time step relative to the grid spacing. It determines the time step size required to accurately capture the time-dependent behavior of the flow. It is particularly important in numerical methods that use explicit time integration schemes. In CFD simulations, it is crucial to choose a Courant number that ensures stability and accuracy. If the Courant number is too large, the solution may become unstable, leading to numerical oscillations and incorrect results. On the other hand, if the Courant number is too small, the simulation becomes computationally expensive as it requires smaller time steps to maintain accuracy.

The appropriate Courant number value depends on the specific flow conditions and the numerical method being employed. Typically, for explicit time integration schemes, a Courant number less than or equal to 1 is used to ensure stability. However, in certain cases, higher Courant numbers may be used for better computational efficiency, as long as stability and accuracy are maintained.

4.3.3 Methodology to select time step for CFD simulation

To determine the necessary time interval, one can utilize the size of a representative geometric feature and the characteristic velocity of the fluid flow, usually the velocity at the inlet. The ratio of a length measurement to velocity provides an estimate of the time needed for the flow to traverse a distance equivalent to the characteristic length. This time interval should be divided into smaller units in order to define the appropriate time step. [12]

For example: Flow over cylinder case used for validation in the current has domain length, L = 0.4 m and cylinder diameter, d = 0.01m, for Re = 100 the u = 0.1571 m/sec considering air at 300K.

Therefore,

$$\text{Flow through time} = \frac{L}{u} = \frac{0.4}{0.1571} = 2.546 \ sec$$

This is the time taken by a particle of air to travel from inlet to outlet. This time can be considered as the largest time scale of the simulation. Similarly, it is possible to calculate a time scale relative to the cylinder, The flow-through-time would be:

$$\text{Flow through time} = \frac{d}{u} = \frac{0.01}{0.1571} = 0.0636 \ sec$$

Hence, the time step could set to be a subdivision of such time scale, say 0.0063 sec

5. Code Validation

For the reliability and checking the accuracy of the present solutions, the numerical code is validated by running the flow and heat transfer simulation for flow past a circular cylinder case. The domain length, L = 0.4 m and cylinder diameter, d = 0.01m is considered, the results were obtained for 100 < Re < 300 in terms of C_d, St, and Nu and compared with available literature [8] for the results of Re = 100.

Table 2 - Comparison for results of flow over cylinder at Re100

	St	*Cd*	*Nu*
Present	0.1451	1.3341	5.2213
Dalal et al. [8]	0.1587	1.4147	5.3523
H. Kapadia et al. [7]	0.1660	1.3739	5.1891
Lange et al. [9]	0.1656	1.3270	5.2110

Table 3 - Results for flow over cylinder at 100 < Re < 300

Re	*St* (present)	*St* [10]	*Cd* (present)	*Cd* [10]	*Nu* (present)	*Nu* [11]
100	0.145044	0.1569	1.3341	1.3353	5.2303	5.22130
200	0.165765	0.1957	1.3376	1.3365	7.5061	7.21205
300	0.186486	0.2150	1.3412	1.3516	9.3978	8.71199

The comparison for C_d, St, and Nu with literature [7–9] for *Re = 100* is listed in Table 2. the present obtained results are in close agreement with those listed in literature with a mean variation of 6.2% in Strouhal number, 3.25% in drag coefficient and 1.68% in Nusselt number.

The comparison for C_d, St, and Nu with literature [10,11] for 100 < Re <300 is listed in Table 3. The overall heat transfer in terms of Nusselt number (Nu) around a circular cylinder is typically correlated by a power law relationship:

$$Nu = C.Re^m.Pr^n$$

Where, *C, m, n* are constants which depends on Re. (C = 0.683, m = 0.466, and n = 0.333 for 40 < Re < 4000) [11]
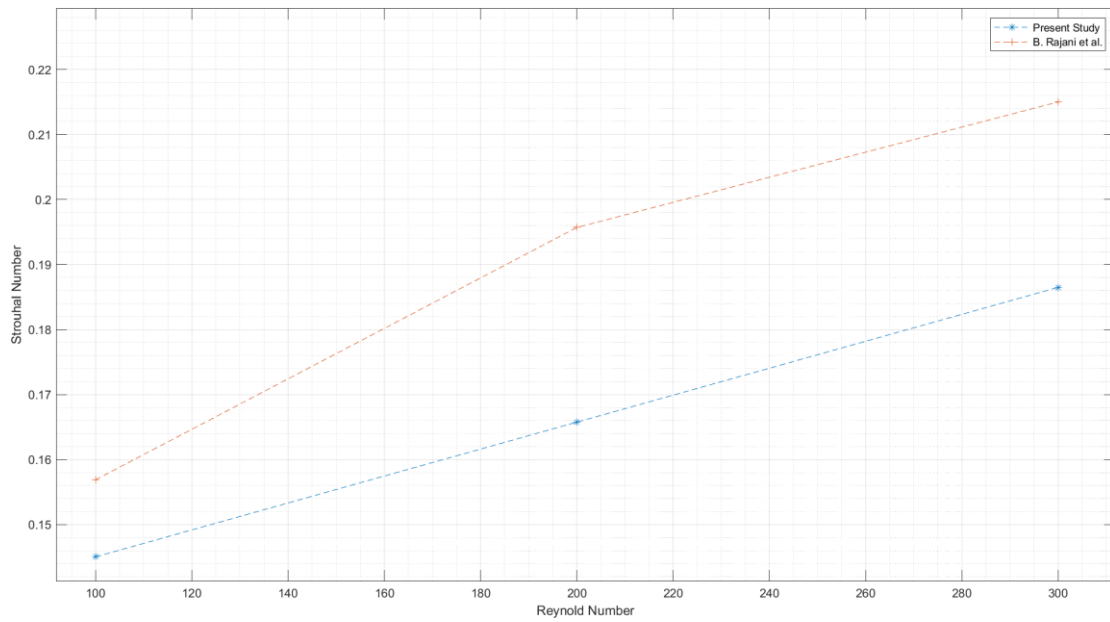
Fig 7 – Variation of Strouhal Number with Re, comparison of present values with results obtained by B. Rajani et al. [10]
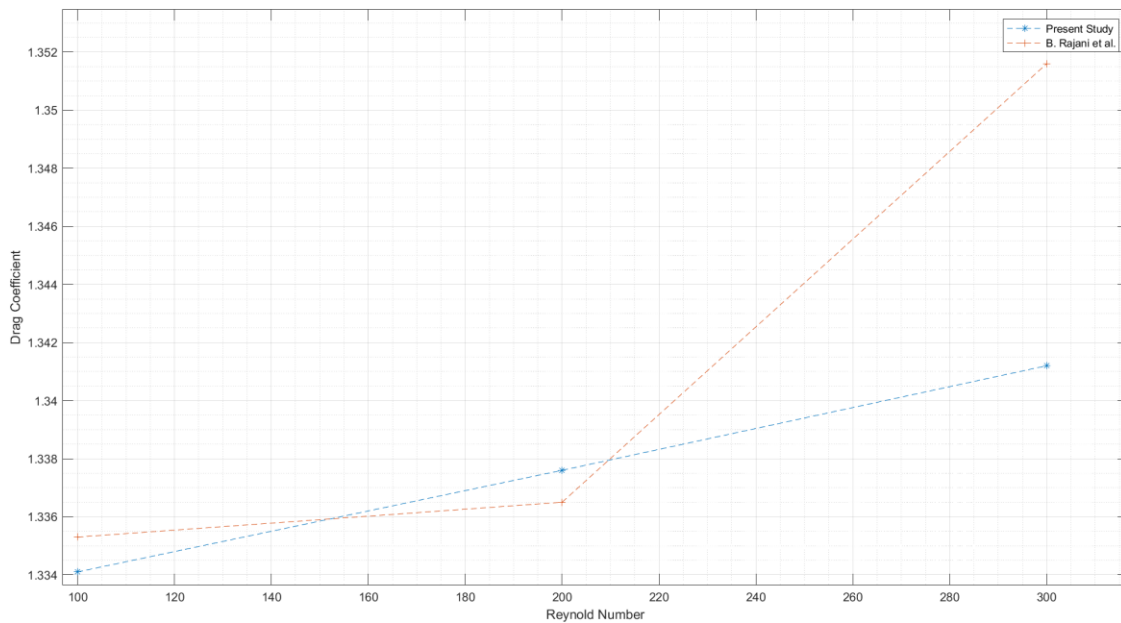
Fig 8 – Variation of Drag coefficient with Re, comparison of present values with results obtained by B. Rajani et al. [10]
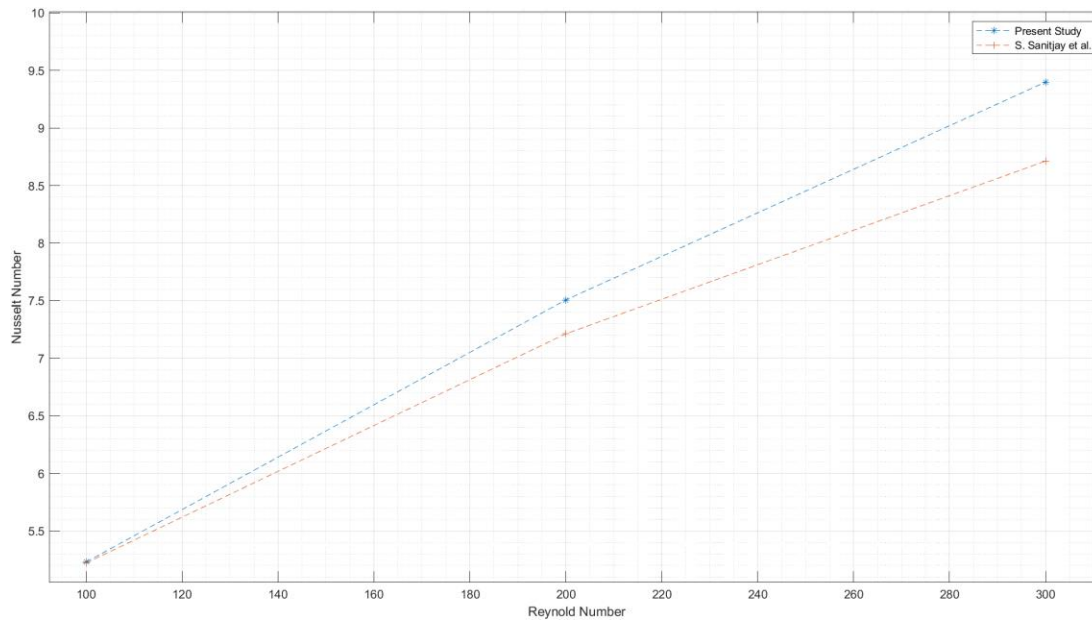
Fig 8 – Variation of Nusselt Number with Re, comparison of present results with correlation from S. Sanitjay et al. [11]

6. Grid Independence Study

The precision of the solution, its convergence, and its numerical stability are all directly influenced by the number of grid points in the computing domain. A fine enough grid is necessary to represent the flow dynamics. However, the computing time grows as the domain's cell count increases. In order to maximize the correctness of the solution and the computational time, a grid independence test is required. In the current work, the grid independence test is run on four grids with increasing levels of refinement. The values of Strouhal number, lift and drag coefficient and Avg. cylinder wall temperature at fixed Re 10000 are contrasted to conduct the grid independence test.

For the present domain, seven different meshes are generated. Table 8 enlists the total number of cells, Strouhal number, coefficient of drag and lift, and Avg. cylinder wall temperature. The M5 has minimal %change of values than compared to M1 – M4, though the %change of values is comparatively less in M6 and M7 but considering the computations economy for the present study M5 is adopted. The Figure 9 shows Variation of lift and drag coefficient & variation of cylinder wall temp. with different Grid size. The Strouhal Number remains constant from M2 – M7. So, for the present computations the grid independence situation is achieved for mesh M5 which can capture the flow physics properly and also be computationally economical.

Table 4 - Grid Independence Study

Mesh	No. of Cells	Cd	%change	CL	%change	Strouhal number	%change	Cylinder wall temp	%change
M1	3180	0.464462193	-	16.4649008	-	0.234375	-	349.989708	-
M2	12720	0.929352135	100.0920955	14.6156061	11.23173909	0.351562	33.33323852	349.956961	0.009357436
M3	23600	0.948198573	2.027911412	15.1583731	3.580641514	0.351562	0	349.949560	0.002114876
M4	52480	1.000443890	5.509955244	13.8554516	9.403674002	0.351562	0	349.963619	0.004017275
M5	94400	0.671682633	32.86153879	14.2164133	2.539049002	0.351562	0	349.953656	0.002846948
M6	146960	0.866141678	28.95103066	14.4964162	1.931531878	0.351562	0	349.933337	0.005806535
M7	209920	0.954359310	10.18512724	14.4068715	0.621541603	0.351562	0	349.929250	0.00116795
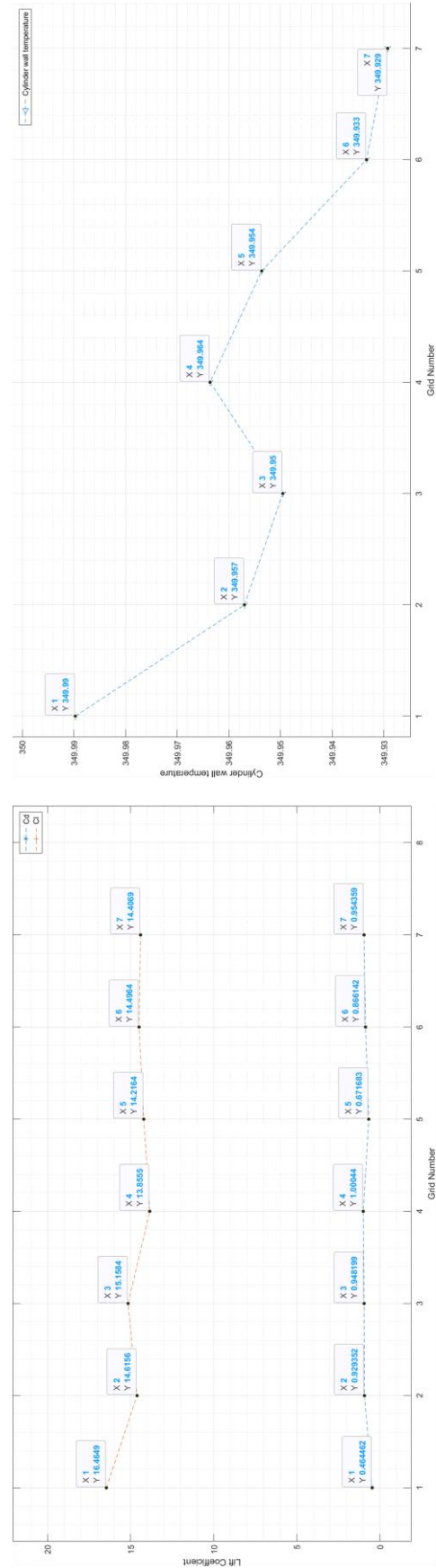
Fig 9 – Variation of lift and drag coefficient (left) & variation of cylinder wall temp. (right) with different Grid size

7. Results and Discussions

For the present study, the fluid flow parameters such as Lift Coefficient, Drag Coefficient, Strouhal Number and heat transfer parameters such as the Nusselt number and The Avg, cylinder wall temperature are of interest. These parameters are obtained for $10^4 < \text{Re} < 10^5$ and logical conclusion have been drawn for variation of all the parameters with Re.

7.1 Lift and Drag Coefficient

The normal and shearing stresses along the lateral and axial directions are what cause the forces to act on the blunt-headed bluff body. While the lift force can be measured along the lateral direction, the drag force can be calculated by projecting this force along the stream-wise direction. The drag and lift acting on the blunt headed body change in the dynamic steady state situation as a result of the intermittent shedding of vortices past it, to counter this, all the values presented are taken at t = 100sec.
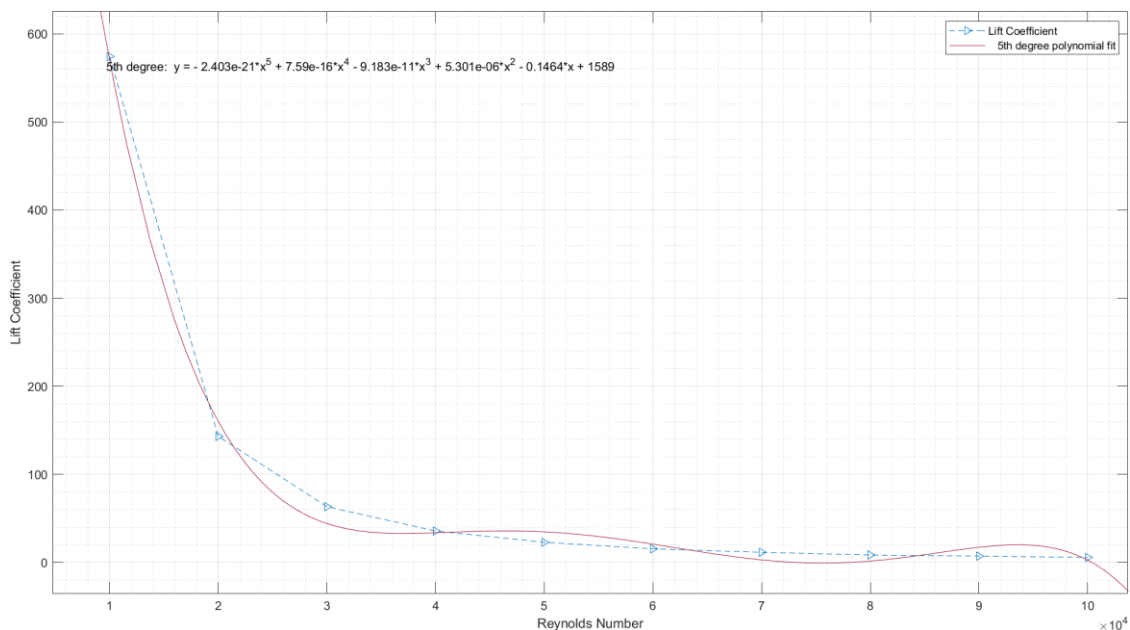
Fig 10 – Variation of Lift Coefficient with Reynolds Number

Figure 10 depicts variation of lift coefficient with Reynolds number, The curve takes a large dip from Re 10000 to Re 20000 and then the curve gets much steeper as Re increase, this can be attributed to several technical reasons. Firstly, as Re increases, the flow becomes more prone to separation, leading to the formation of a recirculation zone behind the cylinder. This reduces the effective lift generation. Secondly, the decreasing boundary layer thickness near the surface of the cylinder reduces the favorable pressure gradient and thus decreases the lift coefficient.

Thirdly, higher Reynolds numbers correspond to more turbulent flow regimes, which disrupt the favorable pressure gradients, increase surface drag, and reduce the lift coefficient. Lastly, as Re increases, the effect of viscosity becomes less significant compared to inertial forces, diminishing the influence of viscous effects on lift generation.
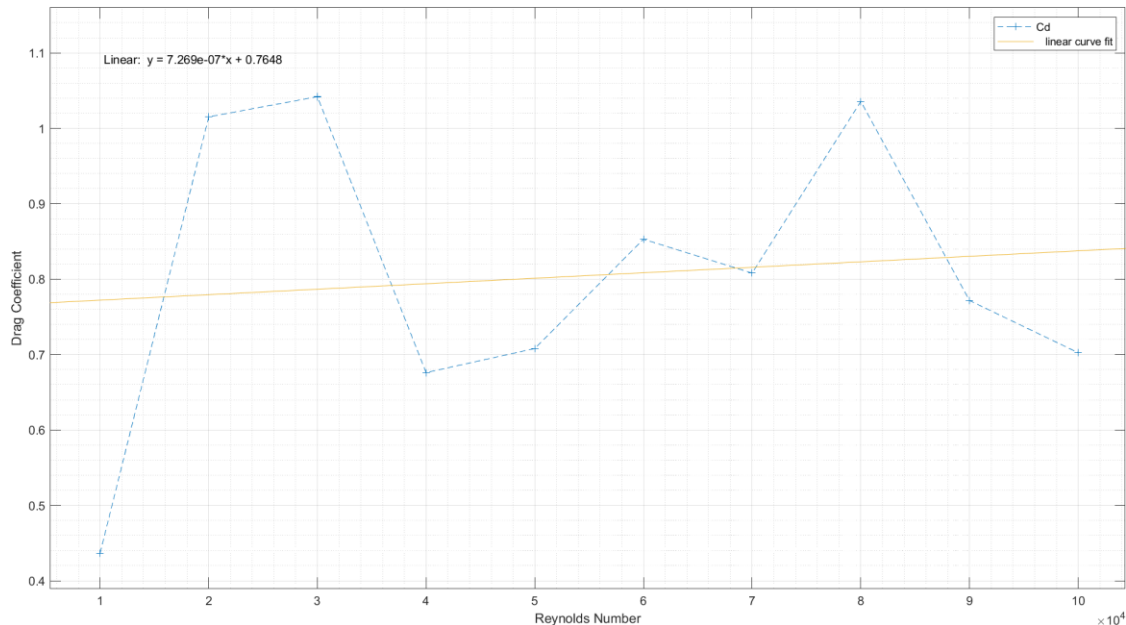
Fig 11 – Variation of drag Coefficient with Reynolds Number

Figure 11 depicts variation of drag coefficient with Reynolds number, The curve follows a chaotic nature with many crests and troughs but when the curve is fitted linearly it is observed that the Cd is increasing with Re. This behavior can be explained by the transition from laminar to turbulent flow, where turbulent flow regimes exhibit higher drag coefficients compared to laminar flow. The decrease in boundary layer thickness and increased turbulence at higher Reynolds numbers contribute to higher skin friction drag and overall drag force on the cylinder. Additionally, flow separation and instabilities that occur at higher Re can lead to increased drag.

7.2 Strouhal Number

The Strouhal number (St) is determined by analyzing the temporal evolution of the lift signal to saturation using the fast Fourier transform (FFT). The FFT generates a plot that represents the energy distribution of various harmonics. The Strouhal number is obtained by identifying the harmonics with the highest energy, as they correspond to the dominant frequency in the lift signal. In other words, the Strouhal number is calculated by selecting the harmonics that

contribute the most to the overall energy content of the lift signal. The python code written to generate and print Strouhal number is given in Annexure 6
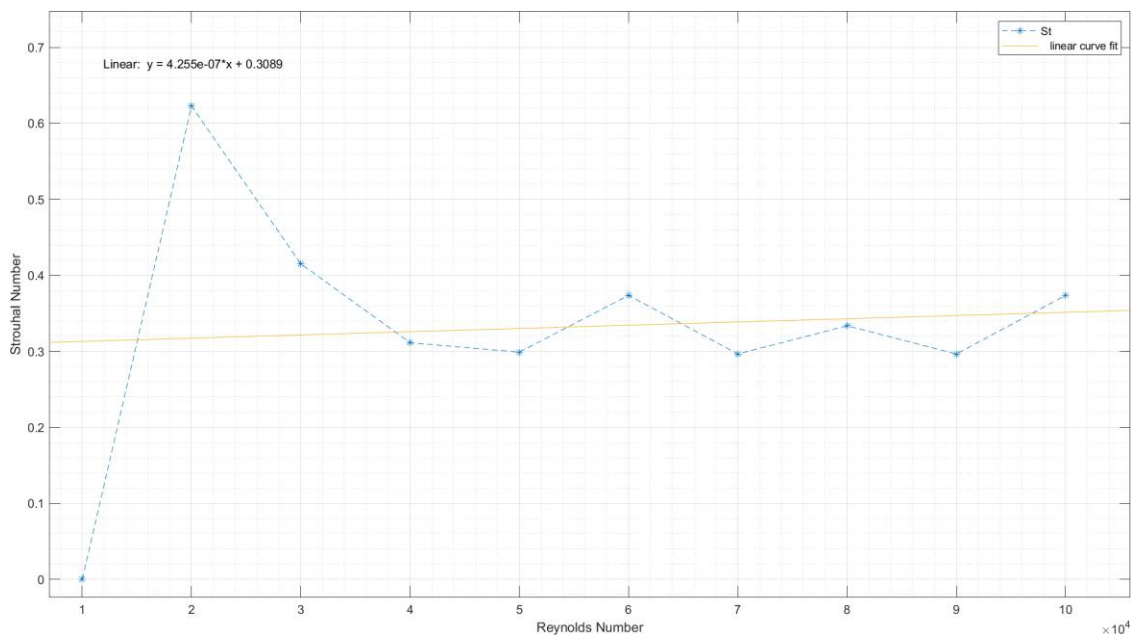
Fig 12 – Variation of Strouhal Number with Reynolds Number

Figure 12 depicts variation of Strouhal number with Reynolds number, it is observed that the Strouhal number output for Re 10,000 is 0. The reason for the Strouhal number being 0 at Re 10,000 could be attributed to the specific flow conditions and characteristics at that particular Reynolds number. The flow behaviour at Re 10,000 might not exhibit distinct and regular vortex shedding patterns or may have an extremely low shedding frequency, leading to a negligible Strouhal number.

Moving on to the observed St curve, the sharp dip between Re 20,000 and Re 50,000 followed by a subsequent rise and fall for the remaining Reynolds numbers can be explained by the transition from laminar to turbulent flow and the phenomenon of vortex shedding.

At lower Reynolds numbers, the flow is typically in the laminar regime, characterized by smooth and predictable flow patterns. In this regime, the shedding of vortices and the associated vortex shedding frequency, which determine the Strouhal number, are relatively low. As the Reynolds number increases, the flow transitions to a turbulent regime, where flow fluctuations and vortex shedding become more prominent.

The sharp dip in the St curve between Re 20,000 and Re 50,000 indicates a transition from laminar to turbulent flow, causing a sudden increase in the shedding frequency and a corresponding decrease in the Strouhal number. As the Reynolds number further increases, the

flow becomes more turbulent, resulting in intensified vortex shedding and higher Strouhal numbers.

When fitting the curve linearly, the increasing trend of the Strouhal number with Reynolds number suggests that the shedding frequency of vortices increases as the Reynolds number increases. This can be attributed to the increased turbulence and stronger vortex shedding in the flow at higher Reynolds numbers.

7.3 Nusselt Number

The heat transfer between the blunt headed body and the free stream of fluid can be represented in terms of the Nusselt number. the Nusselt number helps in understanding how efficiently heat is transferred from the body to the surrounding fluid. A higher Nusselt number indicates enhanced convective heat transfer, implying that the fluid is more effective in carrying away the heat from the body's surface.
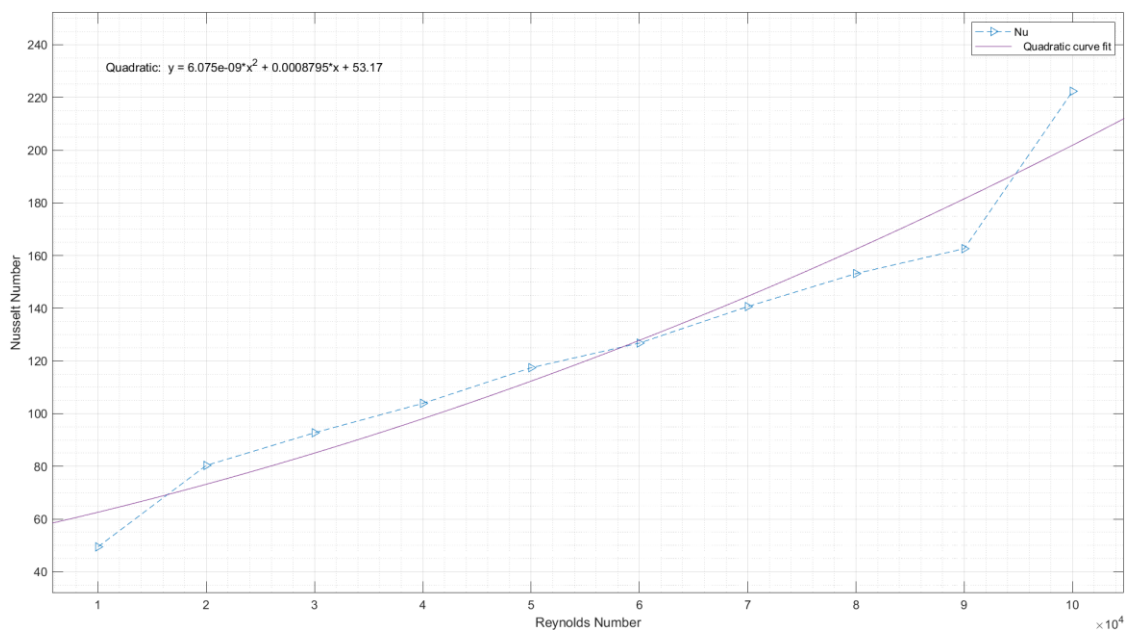
Fig 13 – Variation of Nusselt Number with Reynolds Number

Figure 13 depicts variation of Nusselt number with Reynolds number, it is observed that the Nusselt number increases with increasing Reynolds number.

The increase in the Nusselt number with Re can be attributed to the enhanced convective heat transfer associated with turbulent flow. As the Reynolds number increases, the flow transitions from laminar to turbulent, resulting in increased mixing and flow fluctuations. In turbulent

flow, the fluid moves more vigorously and forms eddies and vortices, leading to better heat transfer between the blunt heated cylinder and the surrounding fluid.

Turbulent flow is characterized by increased momentum and energy transport, which promotes more efficient convective heat transfer. The turbulence enhances the exchange of heat between the surface of the blunt cylinder and the fluid, increasing the convective heat transfer coefficient. Consequently, the Nusselt number, which relates the convective heat transfer to the conductive heat transfer, increases with Re.

7.4 Average cylinder wall temperature

The area average temperature of blunt body wall at t = 100sec are taken into consideration, Figure 14 depicts variation of drag coefficient with Reynolds number, it is observed that with increasing Reynolds number the average temperature of blunt body wall decreases. This can be explained as a result of increasing Nusselt number. the decrease in the average cylinder wall temperature with increasing Reynolds number can be attributed to the enhanced convective heat transfer associated with turbulent flow. The transition from laminar to turbulent flow results in increased fluid motion and mixing near the wall, leading to more efficient heat transfer and lower wall temperatures.
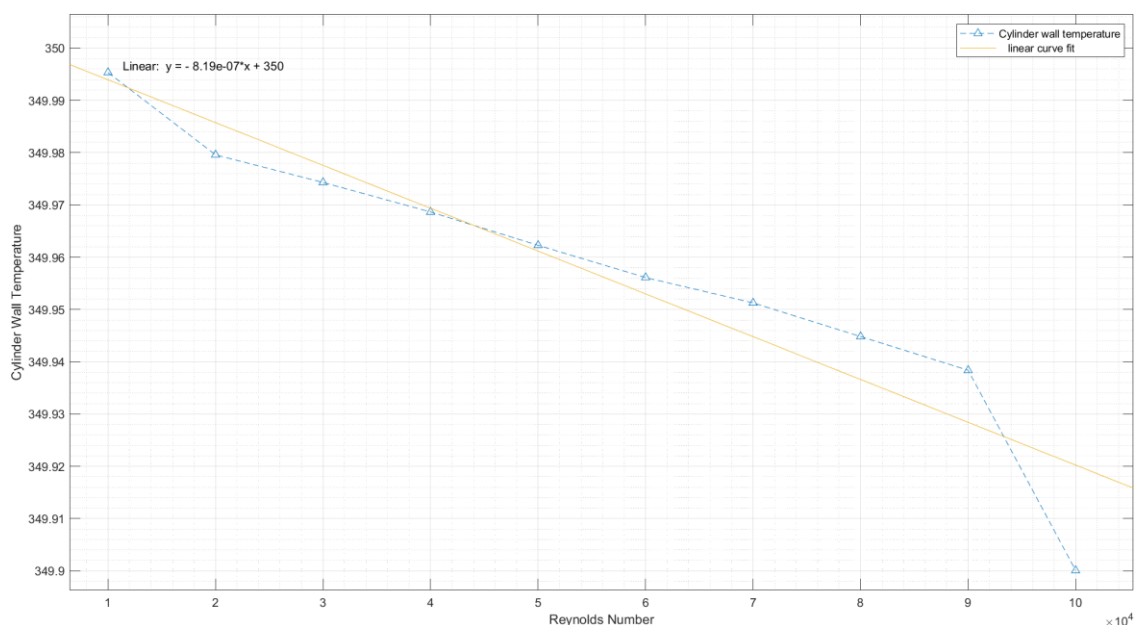
Fig 14 – Variation of cylinder wall temperature with Reynolds Number

The result for with all the fluid flow parameters such as Lift Coefficient, Drag Coefficient, Strouhal Number and heat transfer parameters such as the Nusselt number and The Avg, cylinder wall temperature is enlisted in Table 5

Table 5 – Result Table of blunt heated cylinder for a range of 10000 < Re < 100000

Re	Velocity	time step	Cd	Cl	Shed. Freq.	Strouhal
10000	0.1568	6.377551020E-01	0.43629448	574.3314	-	-
20000	0.3136	3.188775510E-01	1.01519406	143.1530	0.065104	0.622808
30000	0.4704	2.125850340E-01	1.04194192	63.3799	0.130208	0.415205
40000	0.6272	1.594387755E-01	0.67600692	35.7250	0.130208	0.311404
50000	0.7840	1.275510204E-01	0.70793444	22.9632	0.156250	0.298948
60000	0.9408	1.062925170E-01	0.85289125	15.5180	0.234375	0.373685
70000	1.0976	9.110787172E-02	0.80802020	11.5386	0.217014	0.296575
80000	1.2544	7.971938776E-02	1.03565040	8.4891	0.279018	0.333647
90000	1.4112	7.086167800E-02	0.77158820	7.2007	0.279018	0.296575
100000	1.5680	6.377551020E-02	0.70240843	5.7073	0.390625	0.373685

Re	T	Q	h	Nu
10000	349.99534	64.463669	1.2893934	49.438037
20000	349.97958	104.71149	2.0950854	80.32995
30000	349.97432	120.88414	2.4189254	92.746649
40000	349.96865	135.41134	2.7099262	103.90423
50000	349.96228	153.01743	3.0626591	117.42874
60000	349.95612	165.16924	3.3062866	126.76993
70000	349.95128	183.19932	3.6675601	140.62191
80000	349.94483	199.49509	3.9943094	153.15016
90000	349.93839	211.80218	4.2412698	162.61914
100000	349.90009	289.37857	5.7991594	222.35188

7.5 Pressure, Temperature, and Velocity contours

The pressure, temperature, and velocity contours are obtained for 10000 < Re < 100000 These contours provide valuable insights into the flow behaviour, heat transfer characteristics, and fluid dynamics surrounding the blunt cylinder. Here's a brief explanation of the importance of each contour:

Pressure Contours: Pressure contours illustrate the distribution of pressure across the computational domain. They help visualize areas of high and low pressure around the blunt cylinder. Pressure gradients influence the flow pattern, with fluid moving from regions of high pressure to low pressure. The pressure contours can indicate the presence of flow separation,

pressure variations along the cylinder surface, and the formation of pressure gradients that affect the overall flow behaviour.

Temperature Contours: Temperature contours represent the distribution of temperature in the fluid domain. They show the heat transfer patterns and the thermal behaviour of the fluid surrounding the blunt cylinder. Temperature contours help identify regions of heat transfer, such as areas of temperature rise or drop near the cylinder surface. These contours are crucial for understanding the effectiveness of heat transfer from the cylinder to the fluid and can provide insights into the convective heat transfer processes occurring in the flow.

Velocity Contours: Velocity contours display the flow velocities at different locations within the computational domain. They reveal the flow pattern and velocity distribution around the blunt cylinder. Velocity contours help identify regions of flow acceleration, deceleration, and flow separation. They provide a visual representation of the flow structure, such as the formation of vortices, wake regions, and boundary layer development. Velocity contours are essential for understanding the fluid dynamics, including the boundary layer behaviour, flow recirculation zones, and the interaction between the fluid and the blunt cylinder.

By analyzing the pressure, temperature, and velocity contours, a comprehensive understanding of the flow characteristics, heat transfer mechanisms, and fluid behaviour in the vicinity of the blunt heated cylinder can be gained.

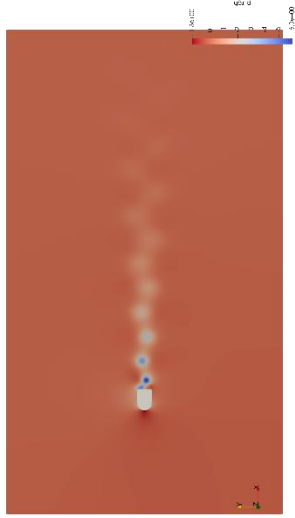| Re	Pressure	Temperature	Velocity
10000			
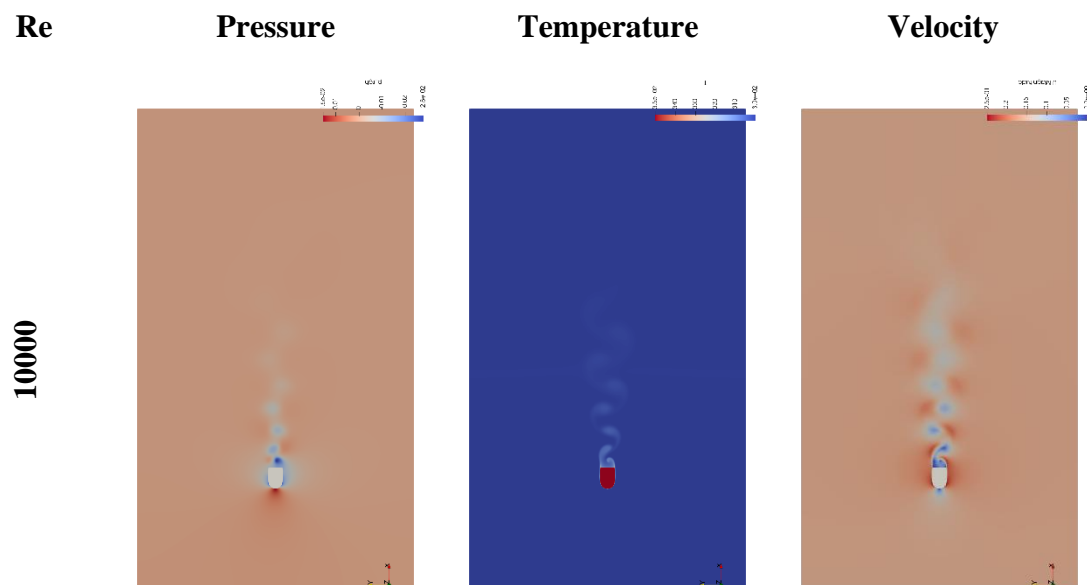
20000
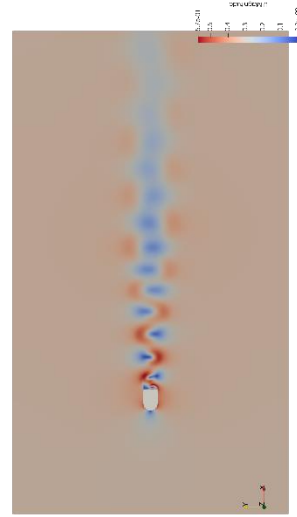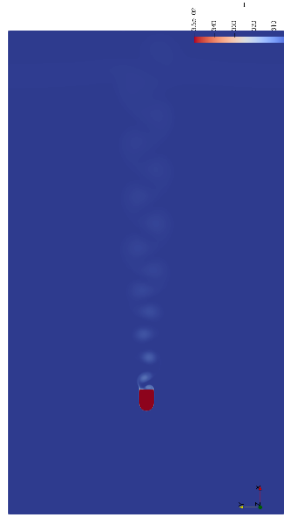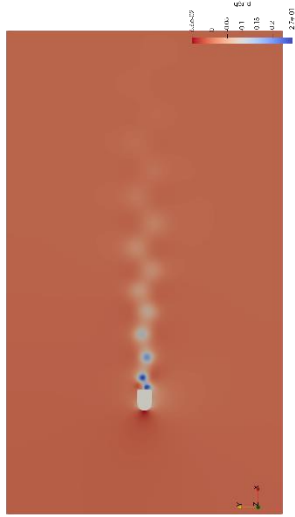
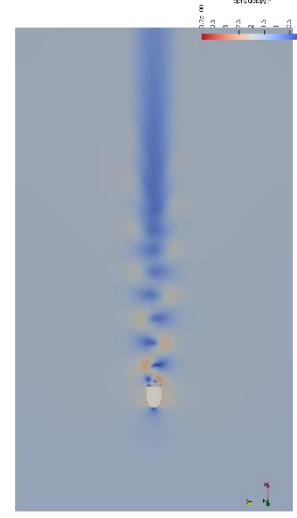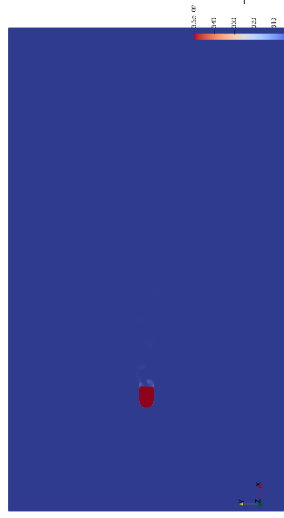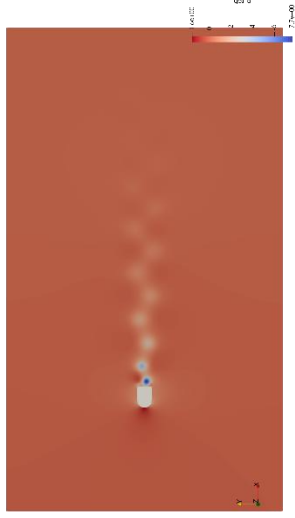**30000**
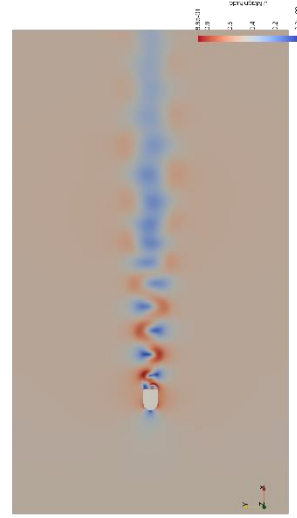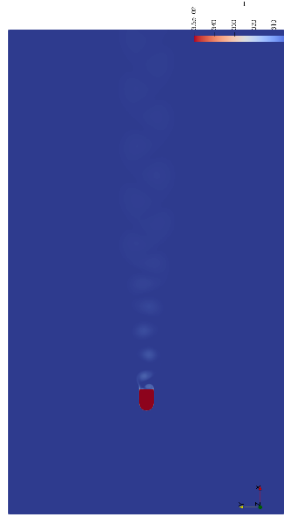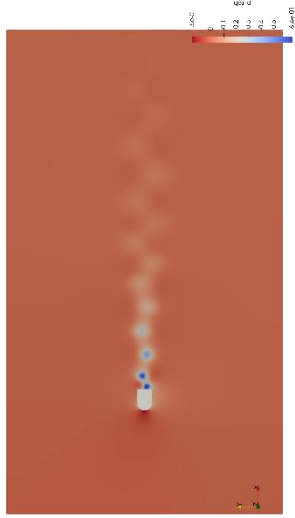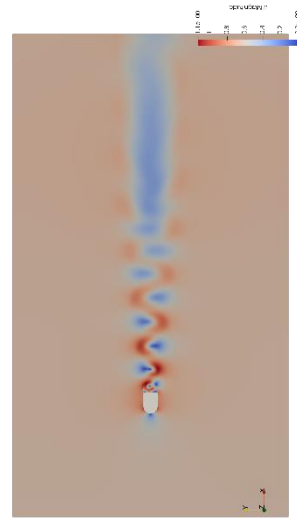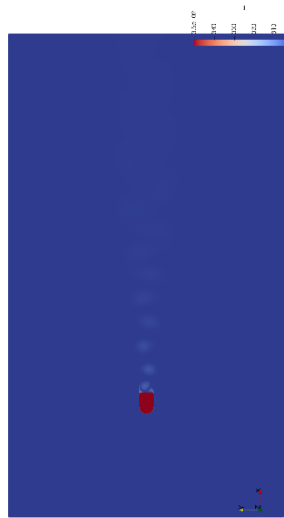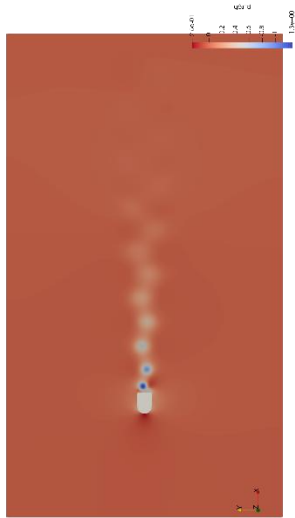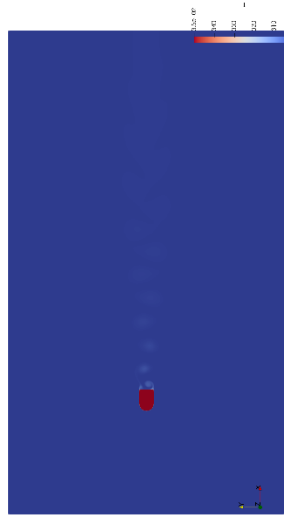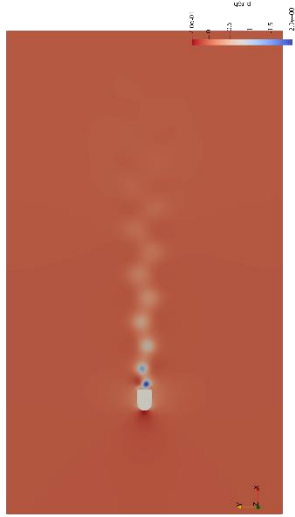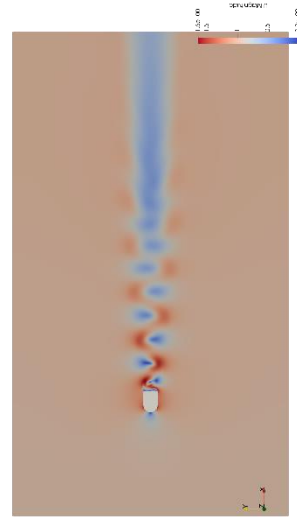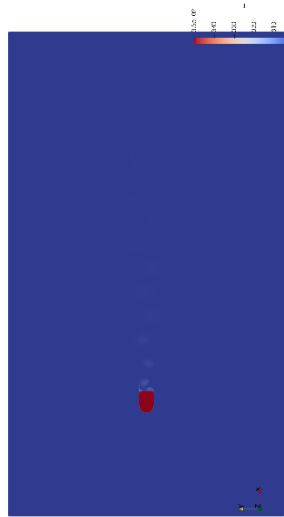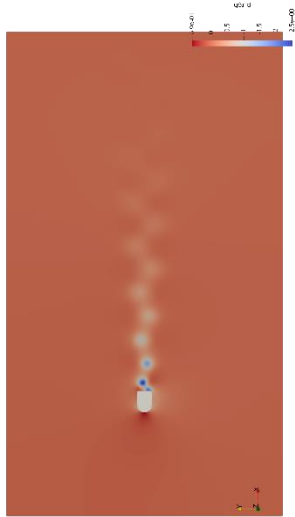
40000
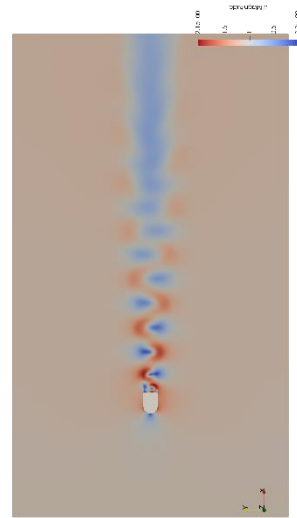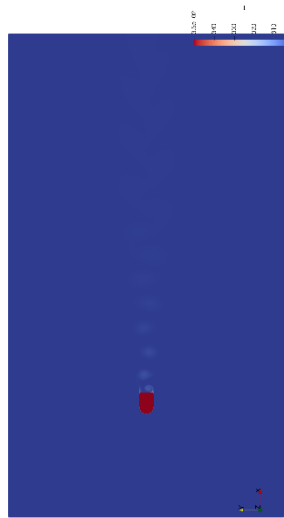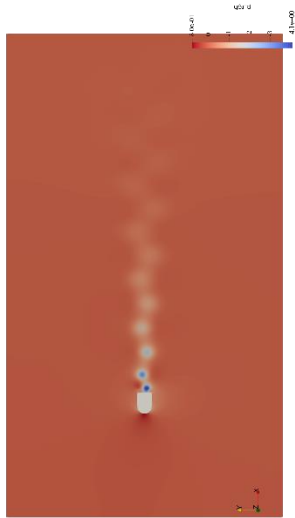
80000
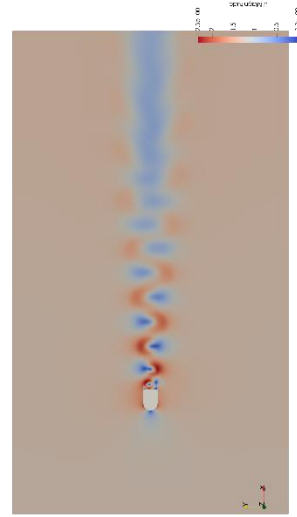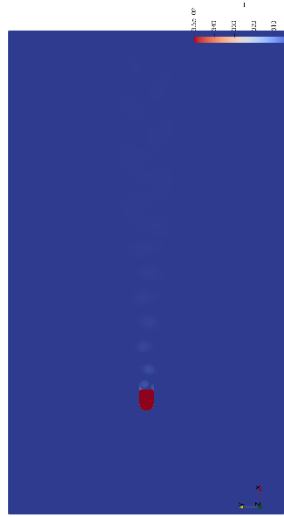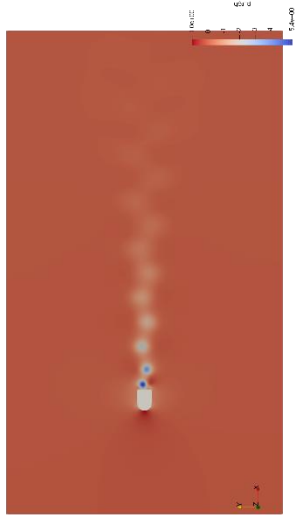
90000
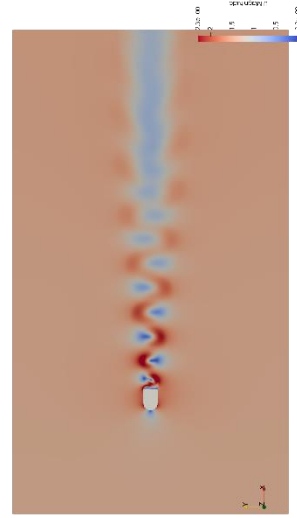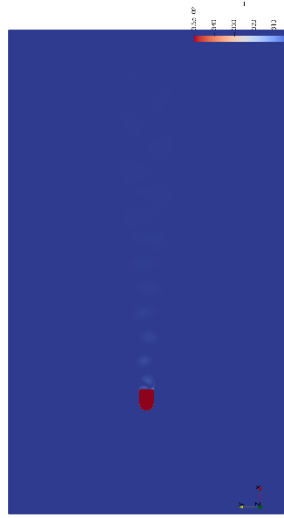
100000

The following observations are made by comparing all the pressure, temperature and velocity contour.

The pressure contours show a high-pressure region on the front face of the blunt cylinder and a low-pressure region on the rear face of the blunt cylinder. The high-pressure region will become more pronounced as the Reynolds number increases. The low-pressure region will also become more pronounced as the Reynolds number increases, but it will be offset from the rear face of the cylinder due to the flow separation. This is due to the Reynolds number increases, the pressure on the front face of the blunt cylinder will increase. This is because the flow will be more turbulent at higher Reynolds numbers, and turbulent flow creates more pressure drag. The pressure on the rear face of the blunt cylinder will decrease as the Reynolds number increases. This is because the flow will separate from the rear face of the cylinder at higher Reynolds numbers, and separated flow creates a low-pressure wake region.

There are no observable changes in temperature contours as the change in initial temperatures set for the solid and fluid region is very less. This is done to ensure the possible physical property changes in the fluid can be neglected.

The velocity contours will show a high-velocity region near the surface of the cylinder and a low-velocity region in the surrounding fluid. The high-velocity region will become wider and more intense as the Reynolds number increases. The low-velocity region will also become wider and more intense as the Reynolds number increases. As the Reynolds number increases, the velocity of the fluid will increase. This is because the turbulent flow will have a higher kinetic energy at higher Reynolds numbers. The velocity of the fluid will also increase near the surface of the cylinder. This is because the turbulent flow will create a boundary layer, and the boundary layer velocity will increase as the Reynolds number increases.

7.6 Variation of C_d and C_l with time

The analysis of lift (Cl) and drag (Cd) coefficient variations over time is important for assessing aerodynamic performance, flow stability, and unsteadiness. The Cl and Cd coefficients provide information about the cylinder's interaction with the flow and its aerodynamic efficiency. Fluctuations in Cl and Cd at higher Reynolds numbers indicate flow unsteadiness and turbulence, caused by vortex shedding in the wake region. Analyzing the fluctuations helps understand flow stability and identify unsteady phenomena affecting the flow field.
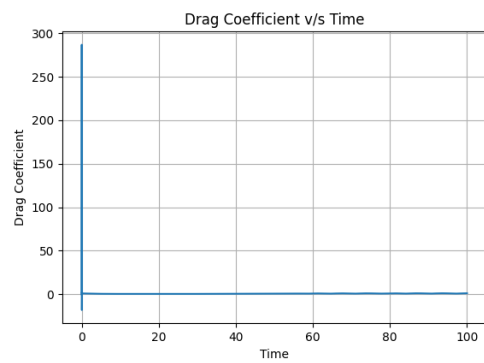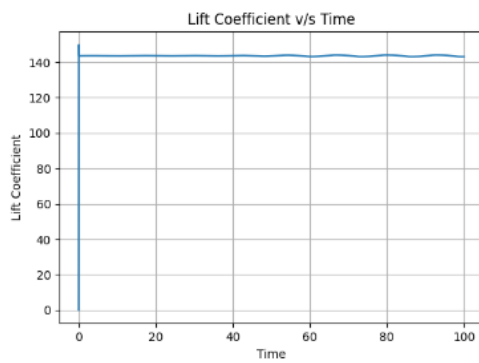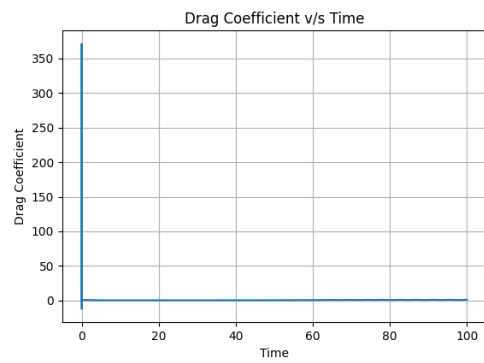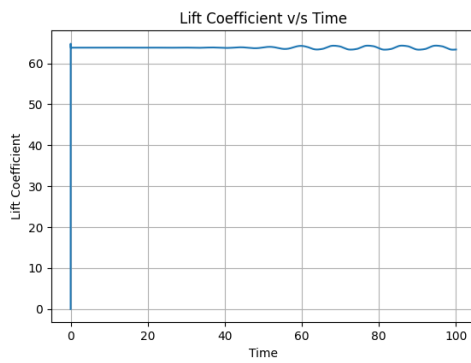
Re	Lift Coefficient	Drag Coefficient

10000

20000

30000

40000

90000

Lift Coefficient v/s Time

Drag Coefficient v/s Time

100000

Lift Coefficient v/s Time

Drag Coefficient v/s Time
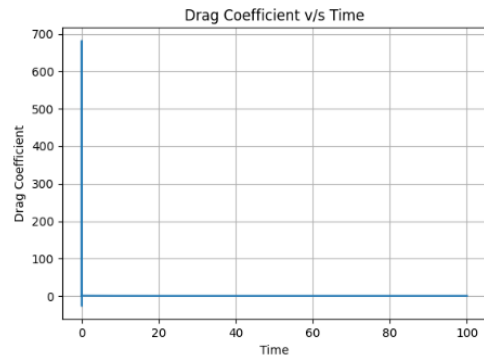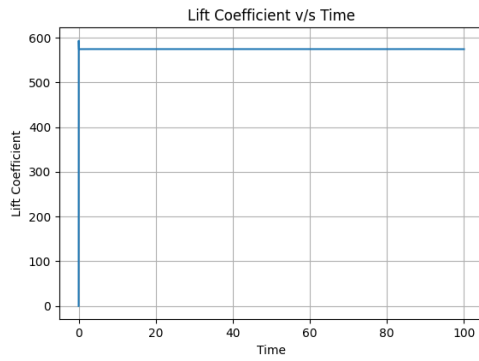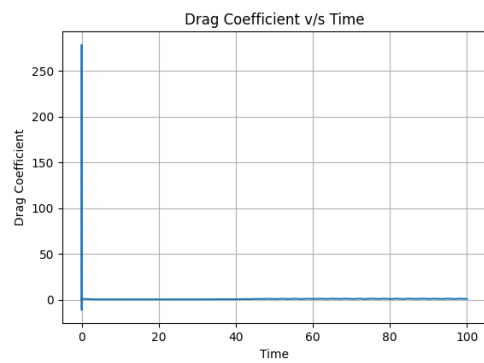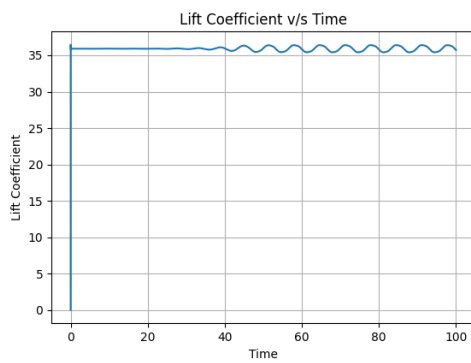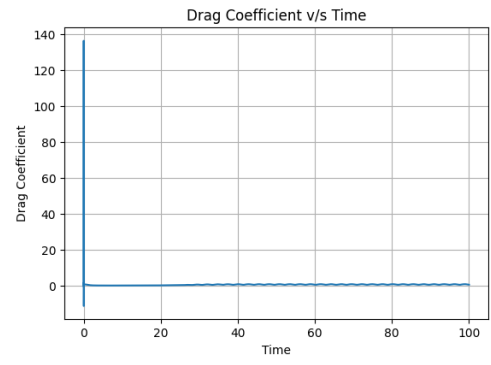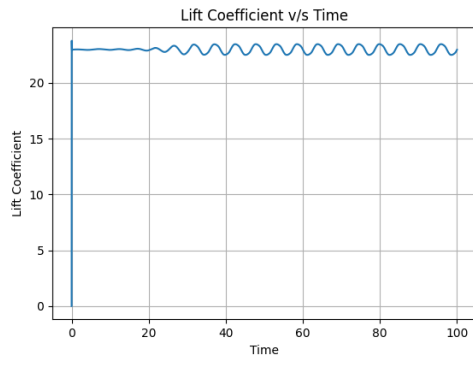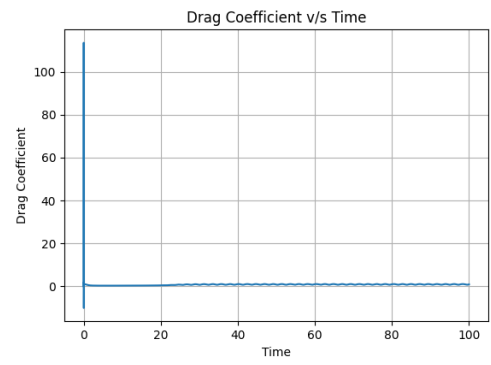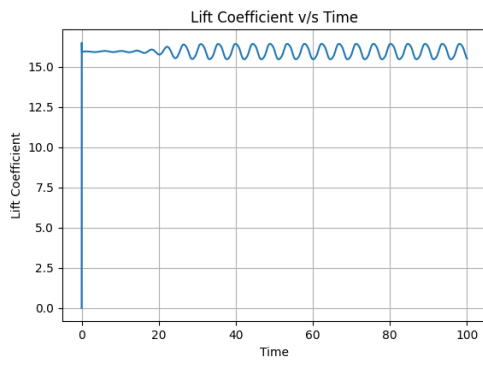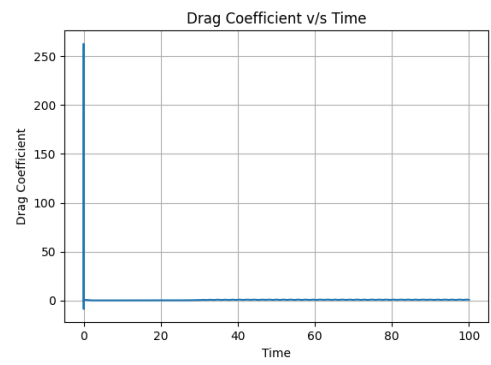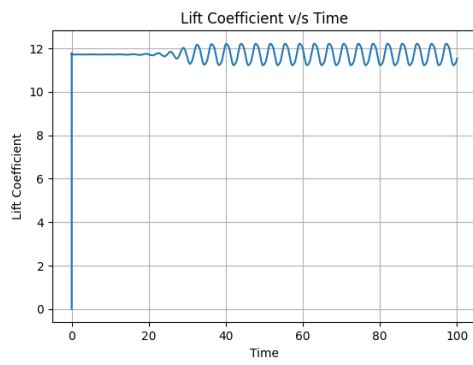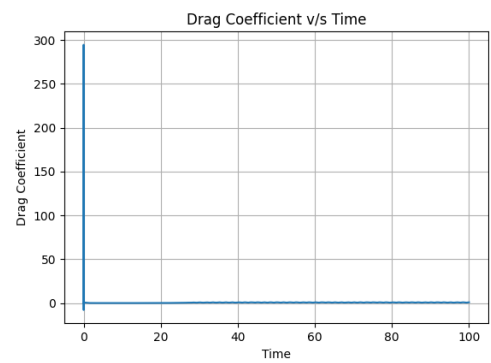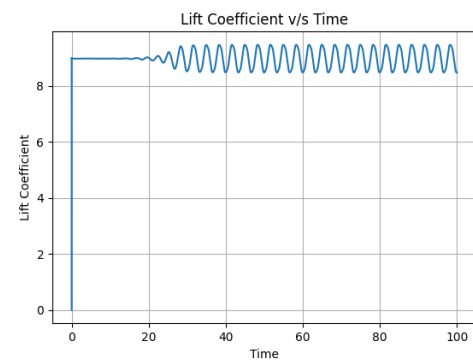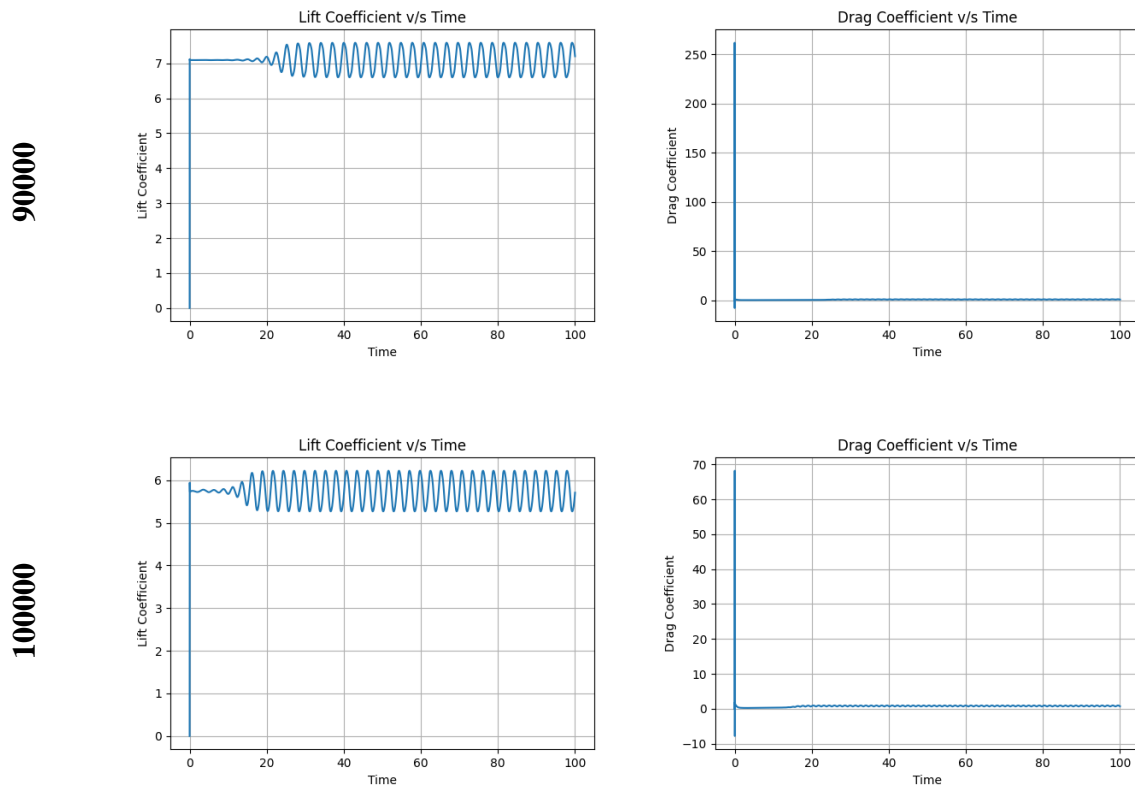
At Reynolds number 10,000, where Cl and Cd remain constant over time, it suggests that the flow is in a steady state. In this case, the flow around the cylinder is likely laminar, resulting in consistent aerodynamic forces. The flow is not exhibiting any significant fluctuations or instabilities, leading to constant Cl and Cd values.

As the Reynolds number increases beyond 10,000, the flow becomes more turbulent and unstable. Turbulence introduces fluctuations and unsteady behaviour in the flow field, which can be observed in the variations of Cl and Cd over time. The fluctuations in Cl and Cd are indicative of the unsteady vortices, flow separation, and transient behaviour occurring in the wake region of the blunt cylinder.

Additionally, it is observed that the formation of fluctuations in the lift (Cl) and drag (Cd) coefficients occurs more rapidly as the Reynolds number (Re) increases. This implies that at higher Re, the flow transitions to a more turbulent regime sooner, leading to faster and more pronounced fluctuations in the Cl and Cd values over time. The increased turbulence intensity at higher Re enhances the shedding of vortices in the wake region, resulting in a more dynamic and unsteady flow behavior.

7.7 Frequency Analysis

The FFT analysis allows to decompose the lift signal into its frequency components. By applying the FFT algorithm, a plot that represents the energy distribution across various harmonics of the signal can be obtained. The harmonics with the highest energy correspond to the dominant frequencies in the lift signal. The Strouhal number (St) can be calculated by identifying the dominant frequency from the FFT plot. The Strouhal number relates the shedding frequency of vortices in the wake of the blunt cylinder to the characteristic flow velocity and the characteristic length of the body.
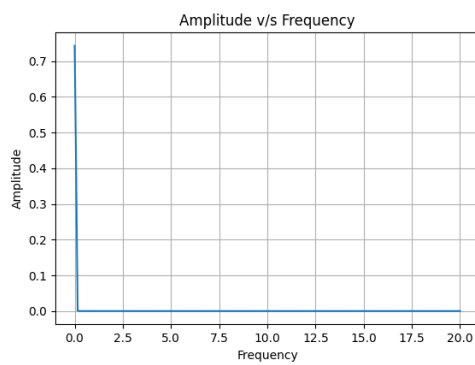
Re 10000
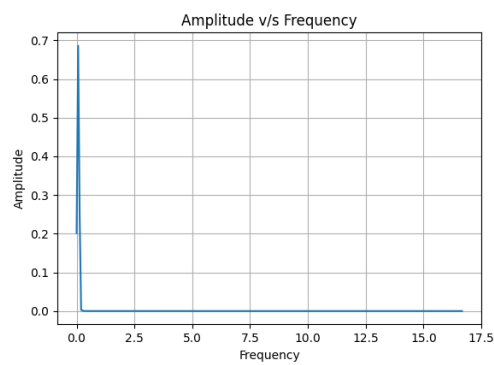
Re 20000
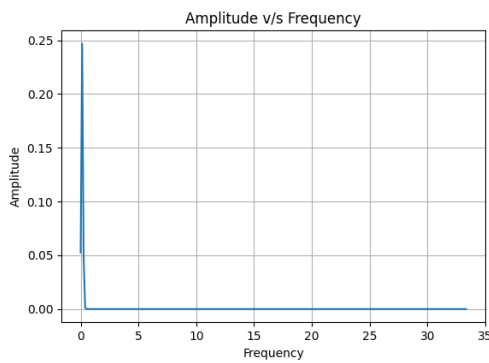
Re 30000
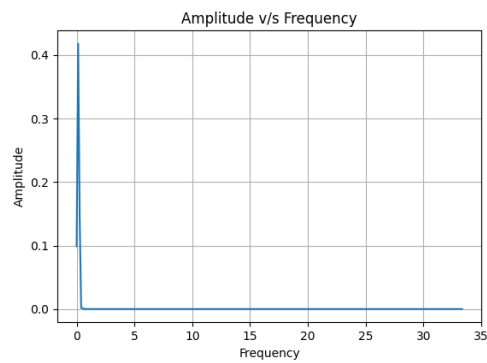
Re 40000
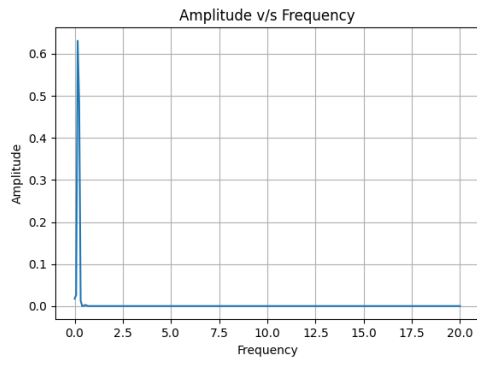
Re 50000
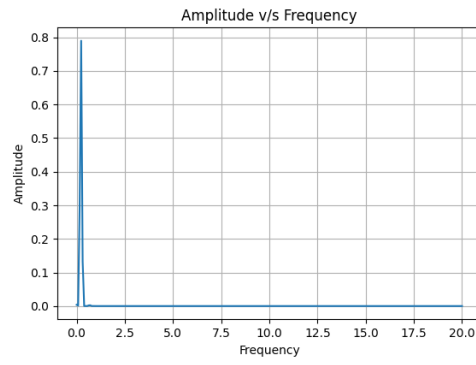
Re 60000
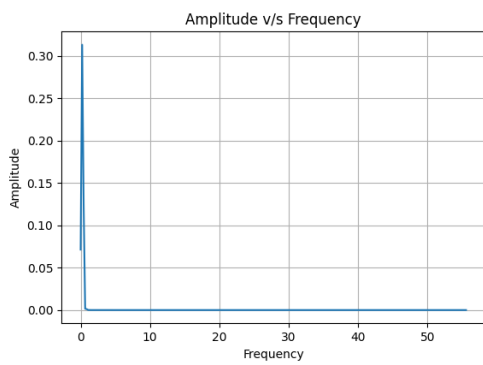
Re 70000
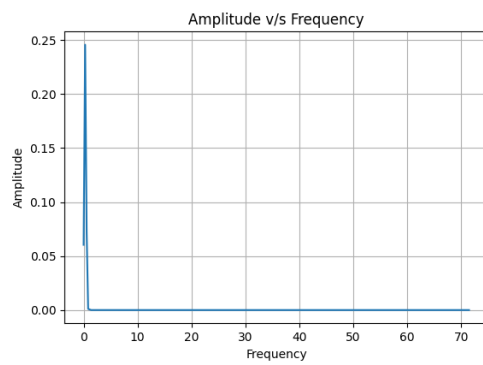
Re 80000
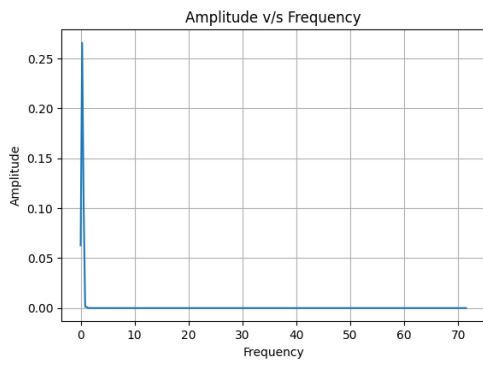
Re 90000
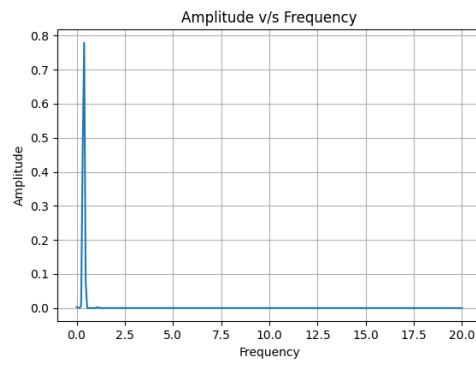
Re 100000
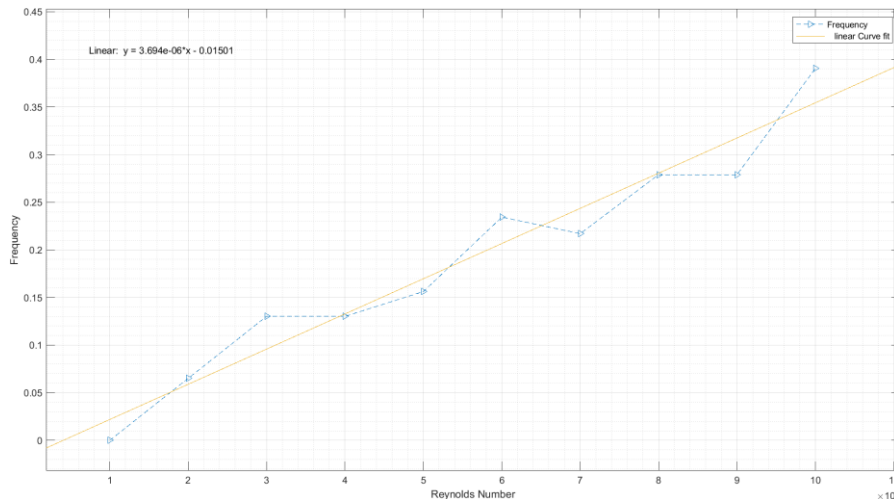
Fig 15 – Variation of frequency obtained from FFT with Reynolds Number

To further analyze the relationship between the dominant frequency and the Reynolds number (Re), the frequency versus Re curve was plotted as shown in Figure 15. The curve shows that the frequency increases with increasing Re, and it exhibits slight fluctuations around the general trend. The technical interpretation of this result is that as the Reynolds number increases, the flow becomes more turbulent and the shedding of vortices in the wake region occurs at a higher frequency. The linear relationship between the frequency and Re suggests that there is a direct correlation between the flow dynamics and the Reynolds number. This behaviour is commonly observed in flow over bluff bodies, where the shedding frequency tends to increase with increasing Reynolds number. The slight fluctuations in the frequency curve can be attributed to the inherent variability in the flow field and the complex interactions between the flow and the cylinder. These fluctuations may be influenced by factors such as flow instabilities, boundary layer effects, and interactions between vortices. However, the overall increasing trend of the frequency with Re indicates that as the flow becomes more turbulent, the vortex shedding occurs at a higher rate.

8. CONCLUSION

The numerical analysis of flow over a blunt heated cylinder using chtMultiRegionFoam in openFOAM yielded valuable insights into the flow behaviour and heat transfer characteristics. The simulation results, presented through pressure, temperature, and velocity contours, provided visual representations of the flow field, enabling a comprehensive understanding of the spatial distribution and behaviour of these parameters.

The study involved analyzing the lift (Cl) and drag (Cd) coefficients over time for Reynolds numbers (Re) ranging from 10000 to 100000. The results revealed that at Re 10000, the coefficients remained constant over time, indicating a steady flow regime. However, at higher Reynolds numbers, fluctuations were observed in the coefficients. These fluctuations indicated the unsteady nature of the flow and were attributed to vortex shedding in the wake region of the cylinder.

To further investigate the vortex shedding phenomenon, the Fast Fourier Transform (FFT) analysis was performed on the lift signal to determine the dominant shedding frequency. This frequency was used to calculate the Strouhal number (St), which represents the shedding frequency relative to other flow parameters. It was observed that the Strouhal number increased with Reynolds number, indicating a higher shedding frequency as the flow became more turbulent.

The heat transfer characteristics were evaluated by analyzing the variation in the Nusselt number (Nu) with Reynolds number. The Nusselt number provides insights into the heat transfer between the cylinder's surface and the surrounding fluid. The study revealed that as the Reynolds number increased, the Nusselt number also increased, indicating enhanced heat transfer from the cylinder.

The analysis of pressure, temperature, and velocity contours provided additional understanding of the flow characteristics. Higher Reynolds numbers resulted in stronger pressure gradients, higher fluid velocities, and changes in temperature distribution. These flow characteristics were influenced by phenomena such as flow separation, boundary layer effects, and vortex shedding.

In conclusion, the study highlighted the influence of Reynolds number on the flow behaviour, heat transfer, and aerodynamic performance of a blunt heated cylinder. The observed fluctuations in lift and drag coefficients, the increasing Strouhal number with Reynolds number, and the enhanced heat transfer at higher Reynolds numbers provided valuable insights into the complex fluid dynamics and heat transfer processes involved. These findings have practical implications in engineering applications, including heat exchanger design optimization, aerodynamic system efficiency improvement, and the understanding of bluff body behaviour in different flow regimes. Further refinements in numerical simulations and deeper investigations can lead to more accurate predictions and design improvements in such systems.

References:

[1]   Song D, Kim W, Kwon O-K, Choi H. Vertical and torsional vibrations before the collapse of the Tacoma Narrows Bridge in 1940. J Fluid Mech 2022;949:A11. https://doi.org/10.1017/jfm.2022.748.

[2]   Sahu AK, Chhabra RP, Eswaran V. Effects of Reynolds and Prandtl numbers on heat transfer from a square cylinder in the unsteady flow regime. Int J Heat Mass Transf 2009;52:839–50. https://doi.org/10.1016/j.ijheatmasstransfer.2008.07.032.

[3]   Sharma A, Eswaran V. HEAT AND FLUID FLOW ACROSS A SQUARE CYLINDER IN THE TWO-DIMENSIONAL LAMINAR FLOW REGIME. Numeri Heat Transf A Appl 2004;45:247–69. https://doi.org/10.1080/10407780490278562.

[4]   Dhiman AK, Chhabra RP, Eswaran V. Flow and heat transfer across a confined square cylinder in the steady flow regime: Effect of Peclet number. Int J Heat Mass Transf 2005;48:4598–614. https://doi.org/10.1016/j.ijheatmasstransfer.2005.04.033.

[5]   Paliwal B, Sharma A, Chhabra RP, Eswaran V. Power law fluid flow past a square cylinder: momentum and heat transfer characteristics. Chem Eng Sci 2003;58:5315–29. https://doi.org/10.1016/j.ces.2003.09.010.

[6]   Gupta AK, Sharma A, Chhabra RP, Eswaran V. Two-Dimensional Steady Flow of a Power-Law Fluid Past a Square Cylinder in a Plane Channel: Momentum and Heat-Transfer Characteristics. Ind Eng Chem Res 2003;42:5674–86. https://doi.org/10.1021/ie030368f.

[7]   Kapadia H, Dalal A, Sarkar S. Forced convective flow and heat transfer past an unconfined blunt headed cylinder. Numeri Heat Transf A Appl 2017;72:372–88. https://doi.org/10.1080/10407782.2017.1376967.

[8]   Dalal A, Eswaran V, Biswas G. A finite-volume method for Navier-Stokes equations on unstructured meshes. Numerical Heat Transfer, Part B: Fundamentals 2008;54:238–59. https://doi.org/10.1080/10407790802182653.

[9]   Lange CF, Durst F, Breuer M. Momentum and heat transfer from cylinders in laminar crossflow at $10{-}4 \leqslant Re \leqslant 200$. Int J Heat Mass Transf 1998;41:3409–30. https://doi.org/10.1016/S0017-9310(98)00077-5.

[10]   Rajani BN, Kandasamy A, Majumdar S. Numerical simulation of laminar flow past a circular cylinder. Appl Math Model 2009;33:1228–47. https://doi.org/10.1016/j.apm.2008.01.017.

[11]   Sanitjai S, Goldstein RJ. Forced convection heat transfer from a circular cylinder in crossflow to air and liquids. Int J Heat Mass Transf 2004;47:4795–805. https://doi.org/10.1016/j.ijheatmasstransfer.2004.05.012.

[12]   Website: https://www.idealsimulations.com/resources/courant-number-cfd/

Annexure - 1: blockMesh code to generate geometry and mesh

```
/*--------------------------------*- C++ -*----------------------------------*\
  =========                 |
  \\      /  F ield         | OpenFOAM: The Open Source CFD Toolbox
   \\    /   O peration     | Website:  https://openfoam.org
    \\  /    A nd           | Version:  10
     \\/     M anipulation  |
\*---------------------------------------------------------------------------*/
FoamFile
{
    format      ascii;
    class       dictionary;
    object      blockMeshDict;
}
// * * * * * * * * * * * * * * * * * * * * * * * * * * * * * * * * * * * * * //

convertToMeters 1;

xc1 80;
xc2 100;
xc3 260;
xc4 60; //xc4 = yc2
yc1 58;
yc2 60;
yc3 58;
zc1 1;

//Mesh refinement
xm1 0.2;
xm2 2;
xm3 0.4;

ym1 0.25;
ym2 4;

vertices
(
//back
(-8 -10 0) //0
(27 -10 0) //1
(27  10 0) //2
(-8  10 0) //3
(0 -0.5 0) //4
(1 -0.5 0) //5
(1  0.5 0) //6
(0  0.5 0) //7
(-3 -3 0) //8
( 3 -3 0) //9
( 3  3 0) //10
(-3  3 0) //11
(-8  3 0) //12
(-8 -3 0) //13
(-3 -10 0) //14
( 3 -10 0) //15
(27 -3 0) //16
(27  3 0) //17
( 3 10 0) //18
(-3 10 0) //19

//front
(-8 -10 0.5) //20
(27 -10 0.5) //21
(27  10 0.5) //22
(-8  10 0.5) //23
(0 -0.5 0.5) //24
(1 -0.5 0.5) //25
(1  0.5 0.5) //26
(0  0.5 0.5) //27
(-3 -3 0.5)  //28
( 3 -3 0.5)  //29
( 3  3 0.5)  //30
(-3  3 0.5)  //31
(-8  3 0.5)  //32
```

```
(-8 -3 0.5)  //33
(-3 -10 0.5) //34
( 3 -10 0.5) //35
(27 -3 0.5)  //36
(27  3 0.5)  //37
( 3 10 0.5)  //38
(-3 10 0.5)  //39
);

blocks
(
hex (10 6 5 9 30 26 25 29) ($xc2 $yc2 $zc1) simpleGrading ($xm1 1 1) //0
hex (11 7 6 10 31 27 26 30) ($xc2 $yc2 $zc1) simpleGrading ($xm1 1 1) //1
hex (8 4 7 11 28 24 27 31) ($xc2 $yc2 $zc1) simpleGrading ($xm1 1 1) //2
hex (9 5 4 8 29 25 24 28) ($xc2 $yc2 $zc1) simpleGrading ($xm1 1 1) //3
hex (0 14 8 13 20 34 28 33) ($xc1 $yc1 $zc1) simpleGrading ($xm3 $ym1 1) //4
hex (14 15 9 8 34 35 29 28) ($xc4 $yc1 $zc1) simpleGrading (1  $ym1 1) //5
hex (15 1 16 9 35 21 36 29) ($xc3 $yc1 $zc1) simpleGrading ($xm2  $ym1 1) //6
hex (9 16 17 10 29 36 37 30) ($xc3 $yc2 $zc1) simpleGrading ($xm2 1 1) //7
hex (10 17 2 18 30 37 22 38) ($xc3 $yc3 $zc1) simpleGrading ($xm2  $ym2 1) //8
hex (11 10 18 19 31 30 38 39) ($xc4 $yc3 $zc1) simpleGrading (1  $ym2 1) //9
hex (12 11 19 3 32 31 39 23) ($xc1 $yc3 $zc1) simpleGrading ($xm3 $ym2 1) //10
hex (13 8 11 12 33 28 31 32) ($xc1 $yc2 $zc1) simpleGrading ($xm3 1 1) //11
hex (4 5 6 7 24 25 26 27) ($xc4 $yc2 $zc1) simpleGrading (1 1 1) //12

);

edges
(
arc 4  7  (-0.5 0   0)
arc 24 27 (-0.5 0 0.5)

arc 8  11 (-4 0 0)
arc 11 10 (0 4 0)
arc 10 9  (4 0 0)
arc 9  8  (0 -4 0)

arc 28 31 (-4 0 0.5)
arc 31 30 ( 0 4 0.5)
arc 30 29 ( 4 0 0.5)
arc 29 28 (0 -4 0.5)
);

boundary
(
    outlet
    {
        type patch;
        faces
        (
        (17 2 22 37)
        (16 17 37 36)
        (1 16 36 21)
      );
    }

    inlet
    {
        type patch;
        faces
        (
        (12 32 23 3)
            (13 33 32 12)
        (0 20 33 13)
        );
    }


    topAndBottom
    {
        type wall;
        faces
        (
```

```
            (3 23 39 19)
            (19 39 38 18)
            (18 38 22 2)
            (0 14 34 20)
            (14 15 35 34)
            (15 1 21 35)

        );
    }

    frontAndBack
    {
        type empty;
        faces
        (
                (12 3 19 11)
                (11 19 18 10)
                (10 18 2 17)
                (9 10 17 16)
                (15 9 16 1)
                (14 8 9 15)
                (0 13 8 14)
                (13 12 11 8)
                (8 11 7 4)
                (11 10 6 7)
                (10 9 5 6)
                (9 8 4 5)
                (4 7 6 5)

                (32 23 39 31)
                (31 39 38 30)
                (30 38 22 37)
                (29 30 37 36)
                (35 29 36 21)
                (34 28 29 35)
                (20 33 28 34)
                (33 32 31 28)
                (28 31 27 24)
                (31 30 26 27)
                (30 29 25 26)
                (29 28 24 25)
                (24 27 26 25)
        );
    }
);

mergePatchPairs
(
);

// ********************************************************************* //
```

Annexure - 2: Mesh quality report

```
/*--------------------------------------------------------------------------*\
  =========                 |
  \\      /  F ield         | OpenFOAM: The Open Source CFD Toolbox
   \\    /   O peration     | Website:  https://openfoam.org
    \\  /    A nd           | Version:  10
     \\/     M anipulation  |
\*--------------------------------------------------------------------------*/
Build  : 10-c4cf895ad8fa
Exec   : checkMesh
Date   : Jun 07 2023
Time   : 00:18:17
Host   : "saqlain-Inspiron-3576"
PID    : 8368
I/O    : uncollated
Case   : /home/saqlain/Downloads/FOSSEE_Internship/M/M5
nProcs : 1
sigFpe : Enabling floating point exception trapping (FOAM_SIGFPE).
fileModificationChecking   :   Monitoring   run-time   modified   files   using   timeStampMaster
(fileModificationSkew 10)
allowSystemOperations : Allowing user-supplied system call operations

// * * * * * * * * * * * * * * * * * * * * * * * * * * * * * * * * * * * * * //
Create time

Create polyMesh for time = 0

Time = 0s

Mesh stats
    points:           189954
    internal points:  0
    faces:            378176
    internal faces:   188224
    cells:            94400
    faces per cell:   6
    boundary patches: 4
    point zones:      0
    face zones:       0
    cell zones:       0

Overall number of cells of each type:
    hexahedra:     94400
    prisms:        0
    wedges:        0
    pyramids:      0
    tet wedges:    0
    tetrahedra:    0
    polyhedra:     0

Checking topology...
    Boundary definition OK.
    Cell to face addressing OK.
    Point usage OK.
    Upper triangular ordering OK.
    Face vertices OK.
    Number of regions: 1 (OK).

Checking patch topology for multiply connected surfaces...
    Patch               Faces    Points    Surface topology
    outlet              176      354       ok (non-closed singly connected)
    inlet               176      354       ok (non-closed singly connected)
    topAndBottom        800      1604      ok (non-closed singly connected)
    frontAndBack        188800   189954    ok (non-closed singly connected)

Checking geometry...
    Overall domain bounding box (-8 -10 0) (27 10 0.5)
    Mesh has 2 geometric (non-empty/wedge) directions (1 1 0)
    Mesh has 2 solution (non-empty) directions (1 1 0)
    All edges aligned with or perpendicular to non-empty directions.
    Boundary openness (1.2208638e-18 -3.2963323e-17 -2.60915e-15) OK.
    Max cell openness = 2.4732092e-16 OK.
```

```
    Max aspect ratio = 45.013766 OK.
    Minimum face area = 1.727463e-05. Maximum face area = 0.11123779.  Face area magnitudes OK.
    Min volume = 8.6373149e-06. Max volume = 0.014232432.  Total volume = 350.  Cell volumes OK.
    Mesh non-orthogonality Max: 87.430197 average: 12.165332
   *Number of severely non-orthogonal (> 70 degrees) faces: 244.
    Non-orthogonality check OK.
  <<Writing 244 non-orthogonal faces to set nonOrthoFaces
    Face pyramids OK.
    Max skewness = 1.5506776 OK.
    Coupled point location match (average 0) OK.

Mesh OK.

End
```

Annexure - 3: topoSetDict file

```
/*--------------------------------*- C++ -*----------------------------------*\
  =========                 |
  \\      /  F ield         | OpenFOAM: The Open Source CFD Toolbox
   \\    /   O peration     | Website:  https://openfoam.org
    \\  /    A nd           | Version:  10
     \\/     M anipulation  |
\*---------------------------------------------------------------------------*/
FoamFile
{
    format      ascii;
    class       dictionary;
    object      topoSetDict;
}

// * * * * * * * * * * * * * * * * * * * * * * * * * * * * * * * * * * * * * * //

#include "$FOAM_CASE/system/blockMeshDict"

actions
(
    {
        name    semicircle;
        type    cellSet;
        action  new;

        setFormat raw;

        source  surfaceToCell;
        sourceInfo
        {
            file    "constant/triSurface/semicircle1.stl";
            type    ascii;

        outsidePoints   ((20 0 0.2)); // definition of outside
        includeCut      false;        // cells cut by surface
        includeInside   false;        // cells not on outside of surf
        includeOutside  true;         // cells on outside of surf
        nearDistance    -1;           // cells with centre near surf  (set to -1 if not used)
        curvature       -100;  //0.9; // cells within nearDistance and near surf curvature
                                      //set to -100 if not used
        }
        //cellZone semicircle;
    }

    {
        name    fluid;
        type    cellZoneSet;
        action  new;
        source  setToCellZone;
        sourceInfo { set semicircle; }
    }
);
// ************************************************************************* //
```

Annexure - 4: controlDict file

```
/*--------------------------------*- C++ -*----------------------------------*\
  =========                 |
  \\      /  F ield         | OpenFOAM: The Open Source CFD Toolbox
   \\    /   O peration     | Website:  https://openfoam.org
    \\  /    A nd           | Version:  10
     \\/     M anipulation  |
\*---------------------------------------------------------------------------*/
FoamFile
{
    format      ascii;
    class       dictionary;
    object      controlDict;
}
// * * * * * * * * * * * * * * * * * * * * * * * * * * * * * * * * * * * * * //

application     chtMultiRegionFoam;

startFrom       startTime;

startTime       0;

stopAt          endTime;

endTime         100;

deltaT          0.025;

writeControl    timeStep;

writeInterval   5;

purgeWrite      0;

writeFormat     ascii;

writePrecision  8;

writeCompression off;

timeFormat      general;

timePrecision   6;

runTimeModifiable true;

adjustTimeStep  no;

maxCo           5;

maxDi           200;

maxDeltaT       1;

functions
{
    #includeFunc patchAverage
    (
        funcName=cylinderT,
        region=fluid,
        patch=fluid_to_solid,
        field=T
    )

    #includeFunc patchAverage
    (
        funcName=inletU,
        region=fluid,
        patch=inlet,
        field=U
    )
```

```
    wallHeatFlux1
    {
    type        wallHeatFlux;
    libs        ("libfieldFunctionObjects.so");
    patches     ("fluid_to_solid");
    region      fluid;
    executeControl  writeTime;
    writeControl    writeTime;
    }

    wallHeatTransferCoeff1
    {
    type            wallHeatTransferCoeff;
    libs            ("libfieldFunctionObjects.so");
    patches         ("solid_to_fluid");
    Pr              0.71438;
    Prt             0.85;
    field           T;
    htcModel        fixedReferenceTemperature;
    TRef            300;
    region          fluid;
    executeControl  writeTime;
    writeControl    writeTime;
    }

    areaAverage1
    {
    type            surfaceFieldValue;
    libs            ("libfieldFunctionObjects.so");
    executeControl  writeTime;
    writeControl    writeTime;
    fields          (T wallHeatTransferCoeff wallHeatFlux);
    operation       areaAverage;
    regionType      patch;
    name            fluid_to_solid;
    region          fluid;
    surfaceFormat   none;
    writeFields     yes;
    }

    forceCoeffs1
    {
    type            forceCoeffs;
    libs            ("libforces.so");
    patches         ("fluid_to_solid");
    region          fluid;

    p               p;
    U               U;
    rho             rhoInf;
    rhoInf          1.1785;

    pRef            10^5;

    porosity        no;

    writeFields     yes;

    // Centre of rotation for moment calculations
    CofR            (0.5 0.5 0);

    // Lift direction
    liftDir         (0 1 0);

    // Drag direction
    dragDir         (1 0 0);

    // Pitch axis
    pitchAxis       (0 0 1);

    // Freestream velocity magnitude [m/s]
    magUInf         0.1568;

    // Reference length [m]
```

```
    lRef            1.5;

    // Reference area [m2]
    Aref            1.0;
    }
}

// ********************************************************************* //
```

Annexure - 5: Python code to generate Strouhal Number

```python
#!/usr/bin/python3

import numpy as np
import scipy.signal as signal
import matplotlib.pyplot as plt

# # Read Results
data = np.loadtxt('./postProcessing/fluid/forceCoeffs1/0/forceCoeffs.dat', skiprows=0)

L       = 1.5       # L = D - Diameter
V       = 0.1568    # Velocity
time    = data[:,0]
Cd      = data[:,2]
Cl      = data[:,3]

del data

# # Compute FFT
N       = len(time)
dt      = time[2] - time[1]

# #Better stable FFT
nmax=512                        # no. of points in the fft
freq, Cd_amp = signal.welch(Cd, 1./dt, nperseg=nmax)
freq, Cl_amp = signal.welch(Cl, 1./dt, nperseg=nmax)
plt.plot(freq, Cl_amp)
plt.grid()
plt.title("Amplitude v/s Frequency")
plt.xlabel("Frequency")
plt.ylabel("Amplitude")
plt.show()

# # Strouhal Number
# Find the index corresponding to max amplitude
Cl_max_fft_idx = np.argmax(abs(Cl_amp))
freq_shed       = freq[Cl_max_fft_idx ]
St              = freq_shed * L / V

print ("Vortex shedding freq: %.6f [Hz]" % (freq_shed))
print ("Strouhal Number: %.6f" % (St))

# # Time v/s Lift Coeff
plt.plot(time,Cl)
plt.grid()
plt.title("Lift Coefficient v/s Time")
plt.xlabel("Time")
plt.ylabel("Lift Coefficient")
plt.show()

# # Time v/s Drag Coeff
plt.plot(time,Cd)
plt.grid()
plt.title("Drag Coefficient v/s Time")
plt.xlabel("Time")
plt.ylabel("Drag Coefficient")
plt.show()
```

51

Annexure - 6: Python code to generate plot of parameters over time

```python
#!/usr/bin/python3

import numpy as np
import scipy.signal as signal
import matplotlib.pyplot as plt

# # Read Results
data = np.loadtxt('./postProcessing/fluid/areaAverage1/0/surfaceFieldValue.dat', skiprows=0)

time    = data[:,0]
Temp    = data[:,1] # Average cylinder wall temp.
hf      = data[:,2] # Average heat transfer coeff
Q       = data[:,3] # Average heat flux

del data

# # Time v/s Average cylinder wall temperature
plt.plot(time,Temp)
plt.grid()
plt.title("Average cylinder wall temperature v/s Time")
plt.xlabel("Time")
plt.ylabel("Average cylinder wall temperature")
plt.show()

# # Time v/s Average heat transfer coeff
plt.plot(time,hf)
plt.grid()
plt.title("Average heat transfer Coefficient v/s Time")
plt.xlabel("Time")
plt.ylabel("Average heat transfer coefficient")
plt.show()

# # Time v/s Average heat flux
plt.plot(time,Q)
plt.grid()
plt.title("Average heat flux v/s Time")
plt.xlabel("Time")
plt.ylabel("Average heat flux")
plt.show()
```

Annexure - 7: Allrun file

```
#!/bin/sh
cd ${0%/*} || exit 1     # Run from this directory

# Source tutorial run functions
. $WM_PROJECT_DIR/bin/tools/RunFunctions

runApplication blockMesh

runApplication checkMesh

runApplication transformPoints "translate=(0.5 0.5 0)"

runApplication topoSet

runApplication splitMeshRegions -cellZones -defaultRegionName solid -overwrite

paraFoam -region fluid -touch
paraFoam -region solid -touch

runApplication $(getApplication)

#------------------------------------------------------------------------------
```